

Numerical Analysis of Nodal Sets for Eigenvalues of Aharonov–Bohm Hamiltonians on the Square with Application to Minimal Partitions

V. Bonnaillie-Noël and B. Helffer

CONTENTS

- 1. Introduction
- 2. Numerical Implementation
- 3. A Few Theoretical Comparison Theorems
- 4. Behavior of the Eigenvalues on the Double Covering of the Punctured Square When Moving the Pole
- 5. Moving the Pole along the Symmetry Axis
- 6. Nodal Sets and Minimal Partitions
- 7. Conclusion
- Acknowledgments
- References

This paper is devoted to presenting numerical simulations and a theoretical interpretation of results for determining the minimal k -partitions of a domain Ω as considered in [Helffer et al. 09]. More precisely, using the double-covering approach introduced by B. Helffer, M. and T. Hoffmann-Ostenhof, and M. Owen and further developed for questions of isospectrality by the authors in collaboration with T. Hoffmann-Ostenhof and S. Terracini in [Helffer et al. 09, Bonnaillie-Noël et al. 09], we analyze the variation of the eigenvalues of the one-pole Aharonov–Bohm Hamiltonian on the square and the nodal picture of the associated eigenfunctions as a function of the pole. This leads us to discover new candidates for minimal k -partitions of the square with a specific topological type and without any symmetric assumption, in contrast to our previous works [Bonnaillie-Noël et al. 10, Bonnaillie-Noël et al. 09]. This illustrates also recent results of B. Noris and S. Terracini; see [Noris and Terracini 10]. This finally supports or disproves conjectures for the minimal 3- and 5-partitions on the square.

1. INTRODUCTION

1.1. Minimal Partitions

For a given partition \mathcal{D} of an open set Ω by k disjoint open subsets D_i , we consider

$$\Lambda(\mathcal{D}) = \max_{i=1,\dots,k} \lambda(D_i),$$

where $\lambda(D_i)$ is the ground-state energy of the Dirichlet Laplacian on D_i . We denote the infimum of Λ over all k -partitions of Ω by

$$\mathfrak{L}_k(\Omega) = \inf_{\mathcal{D} \in \mathcal{D}_k} \Lambda(\mathcal{D}).$$

We look for minimal k -partitions, i.e. partitions $\mathcal{D} = (D_1, \dots, D_k)$ such that

$$\mathfrak{L}_k(\Omega) = \Lambda(\mathcal{D}).$$

We recall that these minimal k -partitions, whose existence was proven in [Conti et al. 03, Conti et al. 05b, Conti et al. 05a], share with nodal domains many properties of regularity, except that the number of half-lines meeting (with equal angle) at critical points of their boundary set can be odd [Helffer et al. 09]. Here by critical points we mean points that are at the intersection of at least three distinct ∂D_i 's. Moreover, it was shown in [Helffer et al. 09] that if all these numbers are even, then the k -minimal partition indeed consists of the k -nodal domains of some eigenfunction of the Dirichlet Laplacian in Ω .

In [Bonnaillie-Noël et al. 10], we combined results of [Helffer et al. 09] and [Helffer et al. 10] with efficient numerical computations to exhibit some candidates for minimal 3-partitions for the square, the disk, etc. This approach was based on the assumption that the minimal 3-partition should inherit from one of the symmetries of the domain. This permits a reduction to a more standard spectral analysis and consequently can give only symmetric candidates. Using two different symmetries of the square, we get the surprise of finding two candidates \mathcal{D}_1 and \mathcal{D}_2 with $\Lambda(\mathcal{D}_1) = \Lambda(\mathcal{D}_2) (\approx 66.581)$ and give numerical evidence that the unique critical point for these partitions is at the center of the square. These candidates are represented in Figure 1(a).

This leads naturally to questions of isospectrality, which were solved using the Aharonov–Bohm Hamiltonian with a singularity at the center of the square; see [Bonnaillie-Noël et al. 09]. This kind of argument also appears in a similar context in [Levitin et al. 06] and [Jakobson et al. 06]. Use of this operator could provide new asymmetric candidates for the 3-minimal partition (see Figure 1(b)), and it is one of the aims of this paper to exhibit them.

1.2. Aharonov–Bohm Hamiltonian

Let us recall some definitions and results about the Aharonov–Bohm Hamiltonian (**ABX**-Hamiltonian for short) with a singularity at X introduced in [Bonnaillie-Noël et al. 09, Helffer et al. 99] and motivated by [Berger and Rubinstein 99]. We denote by $X = (x_0, y_0)$ the coordinates of the pole and consider the magnetic potential with renormalized flux

$$\frac{\Phi}{2\pi} = \frac{1}{2}$$

at X :

$$\begin{aligned} \mathbf{A}^X(x, y) &= (A_1^X(x, y), A_2^X(x, y)) \\ &= \frac{1}{2} \left(-\frac{y - y_0}{r^2}, \frac{x - x_0}{r^2} \right). \end{aligned}$$

We know that the magnetic field vanishes identically in $\dot{\Omega}_X$. The **ABX**-Hamiltonian is defined by considering the Friedrichs extension starting from $C_0^\infty(\dot{\Omega}_X)$, and the associated differential operator is

$$-\Delta_{\mathbf{A}^X} := (D_x - A_1^X)^2 + (D_y - A_2^X)^2$$

with

$$D_x = -i\partial_x \quad \text{and} \quad D_y = -i\partial_y.$$

Let K_X be the antilinear operator

$$K_X = e^{i\theta_X} \Gamma,$$

with

$$(x - x_0) + i(y - y_0) = \sqrt{|x - x_0|^2 + |y - y_0|^2} e^{i\theta_X},$$

and Γ the complex conjugation operator $\Gamma u = \bar{u}$. We say that a function u is K_X -real if it satisfies $K_X u = u$. Then the operator $-\Delta_{\mathbf{A}^X}$ preserves the K_X -real functions, and we can consider a basis of K_X -real eigenfunctions. Hence we analyze only the restriction of the **ABX**-Hamiltonian

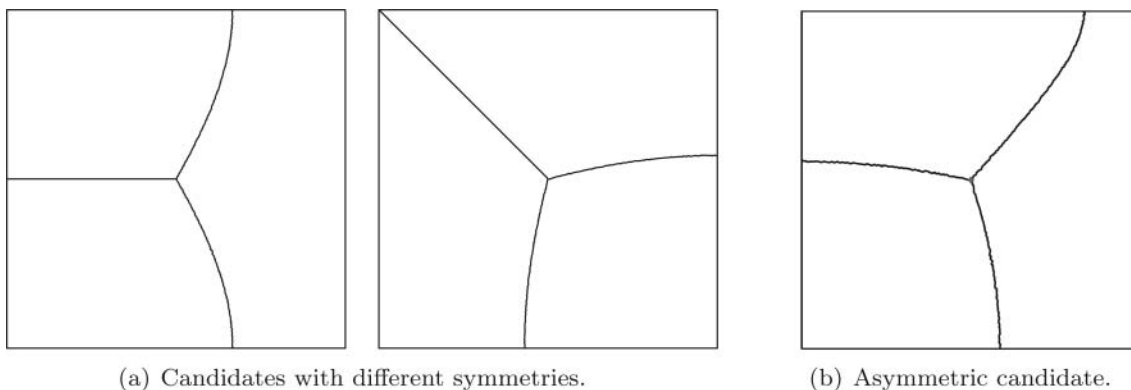


FIGURE 1. Candidates for the minimal 3-partition of the square.

to the K_X -real space $L^2_{K_X}$, where

$$L^2_{K_X}(\dot{\Omega}_X) = \{u \in L^2(\dot{\Omega}_X) \mid K_X u = u\}.$$

It has been shown that the nodal set of such a K_X -real eigenfunction has the same structure as the nodal set of an eigenfunction of the Laplacian, except that an odd number of half-lines should meet at X . When no ambiguity exists, we sometimes omit the reference to X and write more simply θ , K , L^2_K , $-\Delta_A$.

1.3. Main Goals

Although we will return to many of these points in the next sections, let us comment on some of the difficulties we met in this analysis.

As mentioned previously, we have proposed in [Bonnaillie-Noël et al. 10] some symmetric candidates for the minimal 3-partition. If we do not assume a priori symmetries for a minimal 3-partition, a first method, inspired by [Bozorgnia 09], is to test the following iterative method (see [Bonnaillie-Noël and Vial 07]):

Initialization. Let $\mathcal{D}_0 = (D_1^0, D_2^0, D_3^0)$ be a 3-partition of Ω .

Iteration. For $n \geq 1$, we define the partition $\mathcal{D}_n = (D_1^n, D_2^n, D_3^n)$ by:

- $D_1^n = D_3^{n-1}$,
- (D_2^n, D_3^n) is the nodal partition associated to the second eigenvector of the Dirichlet Laplacian on $\text{Int}(\Omega \setminus D_1^n)$.

If the algorithm converges to the partition $\mathcal{D} = (D_1, D_2, D_3)$, then $\Lambda(\mathcal{D}) = \lambda_1(D_1) = \lambda_1(D_2) = \lambda_1(D_3)$. The results obtained in [Bonnaillie-Noël and Vial 07] are at the moment puzzling. Depending on the initial data, the accuracy, and the form of the domain, all possible situations occur: convergence to the candidate, no convergence, convergence to a nonminimal 3-partition. The case of the equilateral triangle is very strange. The authors indeed obtain, for one of the models, convergence to a three-partition whose energy is clearly above the expected energy, whose singular point is at the center of the symmetry, and that is not an eigenvalue of the Aharonov–Bohm Hamiltonian. Another method, followed by [Cybulski et al. 05], also looks interesting, but the paper does not give enough details to permit an analysis of its efficiency.

In any case, admitting that there exists a perfectly good iterative numerical method, it remains interesting

on the mathematical level to see that the obtained candidate for a minimal partition is (or is not) a nodal partition for some Hamiltonian. We will return to this question in the conclusion.

When working on this problem, we realized that we get as a byproduct a nice illustration of the general question of analyzing the deformations of the nodal sets and the transition between different nodal structures when a parameter is varied. There are actually very few theoretical papers on this question, and we also explain the role of the symmetries for solving some questions of avoided crossings or effective crossings; see Section 5.3. This question is very difficult to solve numerically.

We will push a numerical analysis associated with the **ABX**-Hamiltonians with several goals:

- Illustrate the fact that the two symmetric candidates (see Figure 1(a)) for minimal 3-partitions on the square belong actually to a continuous family of not necessarily symmetric candidates (see Figures 1(b) and 8).
- Check, by moving the pole X of the **ABX**-Hamiltonian, the conjecture that the singular point of the minimal 3-partition of the square is at the center.
- Understand and illustrate the mechanism of deformation of the nodal set, and hence extend or guess, in connection with [Noris and Terracini 10], some of the properties described in [Berger and Rubinstein 99] and [Helffer et al. 99] for the ground-state energy (see also [Alziary et al. 03]).

Finally, let us mention that an extended version of this paper, with more computations, is available in [Bonnaillie-Noël and Helffer 09]. We have chosen here to focus on the most interesting phenomena.

1.4. Organization of the Paper

In Section 2, we explain how we implement the computations on the double covering of the punctured square. In Section 3, we apply Courant’s theorem for comparing the eigenvalues of the Dirichlet Laplacian on the square to the Aharonov–Bohm eigenvalues associated with this puncturing. Section 4 analyzes the dependence of the eigenfunctions of the Dirichlet Laplacian on the double covering with respect to the puncturing point. Section 5 is more specifically devoted to an analysis of the behavior of the nodal sets and eigenvalues when the poles belong respectively to the perpendicular bisector $y = \frac{1}{2}$ and the

diagonal $y = x$, which correspond to cases in which some symmetry of the square is respected in the puncturing. We treat also the case of the axis $y = \frac{1}{4} + \frac{x}{2}$ as an example of a generic situation. Section 6 describes the possible applications of our analysis of nodal sets to the research of minimal partitions with a given topological type. We conclude with a presentation of a conjecture motivated by our computations.

2. NUMERICAL IMPLEMENTATION

The **ABX**-Hamiltonian has a singularity at the pole X , and the eigenfunctions are complex-valued. For these reasons, we prefer to deal with the Dirichlet Laplacian on the double covering $\hat{\Omega}_X^{\mathcal{R}}$, whose eigenfunctions are real-valued. Some of these eigenfunctions, which will be described below, are directly related to the K_X -real eigenfunctions of the **ABX**-Hamiltonian, as mentioned in [Bonnaillie-Noël et al. 09, Section 6.3]. For the construction of the double covering, we choose a simple line γ_X joining the pole to the boundary such that $\Omega \setminus \gamma_X$ is simply connected. This path makes it possible to go from one sheet to the other.

The numerical results were realized using the Finite Element Library **MÉLINA** [Martin 07]. The method is completely standard, but the new idea is to work on the double covering of a pointed domain. The computations consist only of the determination of the eigenfunctions of a Dirichlet Laplacian on a double covering domain. Nevertheless, since we are interested in the nodal lines of these eigenfunctions, computations have to be quite accurate, and we chose the package **MÉLINA**, which permits the implementation of high-order elements.

The main point of the numerical part consists in meshing the double covering $\hat{\Omega}_X^{\mathcal{R}}$ of the punctured domain $\Omega \setminus \{X\}$. To do this, we use the two-dimensional mesh generator **TRIANGLE** [Shewchuk 05]. Let us explain in more detail how we proceed.

Let Ω be the square $[0, 1] \times [0, 1]$ and X a point in $[0, \frac{1}{2}] \times [0, \frac{1}{2}]$. We start with meshing the domain Ω so that (see Figure 2):

- the segment joining $(0, 0)$ to the pole X , the dashed line in Figure 2, does not go through any element of the mesh;
- the segment $[(0, 0); X]$ is the union of edges of an even number of triangles;
- the pole X is the vertex of some triangles.

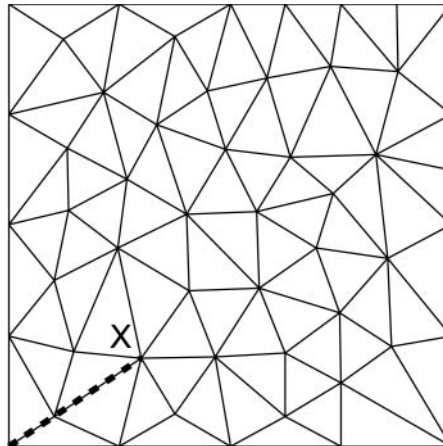


FIGURE 2. Mesh of the double covering $\hat{\Omega}_X^{\mathcal{R}}$.

This first mesh is essentially done for the first sheet, and we repeat this mesh for the second sheet. To obtain a mesh of the double covering $\hat{\Omega}_X^{\mathcal{R}}$, we choose as a cutting line the segment $\gamma_X = [(0, 0); X]$, and we have to exchange the vertex along the segment $[(0, 0); X]$ between the first and second sheets. Then we remove the point X of the second sheet by equating it to the vertex X of the first sheet. For the numerics, X will be chosen on the lattice $\mathcal{P} = \{(\frac{i}{100}, \frac{j}{100}) \mid 1 \leq i, j \leq 50\}$.

Theoretically, the eigenvalues and eigenfunctions depend only on the pole and are independent of the cut chosen for our construction. The introduction of the segment $[(0, 0); X]$ is only a technical point, and we have verified that the numerical computations of the eigenfunctions and eigenvalues are (with a rather good accuracy $\approx 10^{-3}$) independent of the choice of the line joining the pole to the boundary, that is, the line between the first and second sheets.¹ The computed eigenvalues are given throughout this paper within the value $5 \cdot 10^{-4}$.

In the following, we use a \mathbb{P}^6 approximation with at least 6000 elements. To detect the nodal lines, we use a program realized by G. Vial. The idea is that it is very easy to compute the zero set of linear functions. In our case, we deal with a function that is piecewise \mathbb{P}^k and given by a finite element method. We know the values of this function at some points. As soon as we have these values, we can replace this function by a new function that is piecewise linear. For this, we introduce some new

¹Many computations corresponding to two different choices of cutting lines are available on the web page <http://w3.bretagne.ens-cachan.fr/math/simulations/MinimalPartitions/covering.php> (see [Bonnaillie-Noël and Vial 07]).

points by an interpolation method. Then we detect the zero set of this new function.

3. A FEW THEORETICAL COMPARISON THEOREMS

3.1. Notation

We denote by Ω the square $[0, 1] \times [0, 1]$ and by $C = (\frac{1}{2}, \frac{1}{2})$ the center of the square. We compute the eigenfunctions of the Laplacian on the double covering $\dot{\Omega}_X^{\mathcal{R}}$ of $\dot{\Omega}_X = \Omega \setminus \{X\}$. By a symmetry argument, it is enough to consider $X = (x_0, y_0)$ in the quarter square $[0, \frac{1}{2}] \times [0, \frac{1}{2}]$.

There are two ways of labeling the eigenvalues: We can label them in the standard way and then denote by $\lambda_k(\dot{\Omega}_X^{\mathcal{R}})$ the k th eigenvalue of the Dirichlet Laplacian on $\dot{\Omega}_X^{\mathcal{R}}$. We can also take account of the symmetry relative to the deck map $\mathcal{D}_X^{\mathcal{R}}$, which associates with a given point in the covering the distinct point with same projection by the covering map $\pi_X^{\mathcal{R}}$ of $\dot{\Omega}_X^{\mathcal{R}}$ onto $\dot{\Omega}_X$. This splits the spectrum into two independent spectra relative to two orthogonal spaces in $L^2(\dot{\Omega}_X^{\mathcal{R}})$.

The eigenvalues correspond either to

- (1) eigenfunctions lifted from the eigenfunctions (of the Dirichlet Laplacian)² on the square by the covering map (sometimes called $\mathcal{D}_X^{\mathcal{R}}$ -symmetric because they are symmetric with respect to the deck map,
- (2) or to eigenfunctions that are $\mathcal{D}_X^{\mathcal{R}}$ -antisymmetric with respect to the deck map.

We also call them **ABX**-eigenvalues because they can be seen as eigenvalues of an **AB**-Hamiltonian with a pole X creating a renormalized flux equal to $\frac{1}{2}$. We use the shorthand “**ABX**-Hamiltonian” if we want to make explicit the reference to the pole. We denote by $\lambda_j^{\mathbf{AB}X} =$

$\lambda_j^{\mathbf{AB}}(\dot{\Omega}_X)$ the j th eigenvalue of the **AB**-Hamiltonian with pole at X .

In consequence, for any pole X and any integer k , the eigenvalue $\lambda_k(\dot{\Omega}_X^{\mathcal{R}})$ of the Dirichlet Laplacian on the double covering is either an eigenvalue $\lambda_j(\Omega)$ of the square or an eigenvalue $\lambda_j^{\mathbf{AB}X}$ of the **AB**-Hamiltonian on $\dot{\Omega}_X$ with pole at X .

3.2. Eigenvalues of the Square

The eigenvalues of the square are well known and given by the double sequence $\pi^2(m^2 + n^2)$ with $m \in \mathbb{N} \setminus \{0\}$, $n \in \mathbb{N} \setminus \{0\}$, with corresponding basis of eigenfunctions given by

$$\Omega \ni (x, y) \mapsto \phi_{mn}(x, y) := \sin(m\pi x) \sin(n\pi y).$$

Labeling the eigenvalues in increasing order leads to the sequence denoted by $\lambda_k(\Omega)$, $k \in \mathbb{N}^*$. Table 1 gives the first eight eigenvalues and the nodal set of the associated eigenfunctions belonging to the above basis. The second, fifth, and seventh eigenvalues are double, and consequently, it is also natural to look at the nodal sets of linear combinations in order to determine all the possible nodal configurations associated with this eigenvalue.

We note that the $\mathcal{D}_X^{\mathcal{R}}$ -symmetric spectrum of the Dirichlet Laplacian on the double covering $\dot{\Omega}_X^{\mathcal{R}}$ is the spectrum of the square and is independent of the pole. This is a consequence of the fact that the spectra of the Dirichlet Laplacian in Ω and $\dot{\Omega}_X$ are the same, the puncturing point being of capacity 0. So it is more the **ABX**-spectrum that is of interest, because it depends on the position of the pole. Nevertheless, the standard labeling of all the eigenvalues on $\dot{\Omega}_X^{\mathcal{R}}$ can play a role in the application of Courant’s theorem. Of course, we have $\lambda_1(\dot{\Omega}_X^{\mathcal{R}}) = \lambda_1(\Omega)$.

Eigenvalues of the Square	(m, n) -Labeling	Nodal Sets for ϕ_{mn}
$\lambda_1(\Omega) = 2\pi^2 \approx 19.739$	(1, 1)	
$\lambda_2(\Omega) = \lambda_3(\Omega) = 5\pi^2 \approx 49.348$	(2, 1), (1, 2)	
$\lambda_4(\Omega) = 8\pi^2 \approx 78.957$	(2, 2)	
$\lambda_5(\Omega) = \lambda_6(\Omega) = 10\pi^2 \approx 98.696$	(3, 1), (1, 3)	
$\lambda_7(\Omega) = \lambda_8(\Omega) = 13\pi^2 \approx 128.305$	(3, 2), (2, 3)	

TABLE 1. First eight eigenvalues of the Dirichlet Laplacian on Ω and nodal sets for the associated basis ϕ_{mn} .

²We sometimes, for brevity, speak simply of the spectrum of the square.

3.3. Theoretical Estimates of the Eigenvalues

This subsection is concerned with a comparison among the spectrum on the square, the spectrum on the double covering $\dot{\Omega}_X^{\mathcal{R}}$, and the \mathbf{ABX} -spectrum. We propose some equalities and upper bounds between the eigenvalues essentially based on the minimax principle and on Courant’s nodal theorem, which is recalled now.

Theorem 3.1. *Let $k \geq 1$, $\lambda_k(D)$ be the k th eigenvalue for the Dirichlet Laplacian on D . Then any associated eigenfunction has at most k nodal domains.*

We would also like to apply this theorem to the K_X -real eigenfunctions of the \mathbf{ABX} -Hamiltonian on $\dot{\Omega}_X$. Equivalently, this corresponds to a Courant nodal theorem for the $\mathcal{D}_X^{\mathcal{R}}$ -antisymmetric eigenfunctions on $\dot{\Omega}_X^{\mathcal{R}}$, already discussed in [Bonnaillie-Noël et al. 09]. A combination of the Courant nodal theorem and the max–min principle for the \mathbf{ABX} -Hamiltonian leads to the following proposition.

Proposition 3.2. *Let $X \in [0, \frac{1}{2}] \times [0, \frac{1}{2}]$. Then*

$$\lambda_1(\Omega) = \lambda_1(\dot{\Omega}_X^{\mathcal{R}}), \quad \lambda_1^{\mathbf{ABX}} = \lambda_2(\dot{\Omega}_X^{\mathcal{R}}), \quad \lambda_2^{\mathbf{ABX}} = \lambda_3(\dot{\Omega}_X^{\mathcal{R}}), \quad (3-1)$$

and for $k = 2, 4, 5, 7, 9, 11$, there exists an integer ℓ_k such that

$$\lambda_2^{\mathbf{ABX}} < \lambda_2(\Omega) = \lambda_{\ell_2}(\dot{\Omega}_X^{\mathcal{R}}) \text{ with } \ell_2 \geq 4 \quad (3-2)$$

(with multiplicity at least 2),

$$\lambda_3^{\mathbf{ABX}} \leq \lambda_4(\Omega) = \lambda_{\ell_4}(\dot{\Omega}_X^{\mathcal{R}}) \text{ with } \ell_4 \geq 7, \quad (3-3)$$

$$\lambda_5(\Omega) = \lambda_{\ell_5}(\dot{\Omega}_X^{\mathcal{R}}) \text{ with } \ell_5 \geq 8, \quad (3-4)$$

$$\lambda_5^{\mathbf{ABX}} \leq \lambda_7(\Omega) = \lambda_{\ell_7}(\dot{\Omega}_X^{\mathcal{R}}) \text{ with } \ell_7 \geq 12, \quad (3-5)$$

$$\lambda_9(\Omega) = \lambda_{\ell_9}(\dot{\Omega}_X^{\mathcal{R}}) \text{ with } \ell_9 \geq 14, \quad (3-6)$$

$$\lambda_8^{\mathbf{ABX}} \leq \lambda_{11}(\Omega) = \lambda_{\ell_{11}}(\dot{\Omega}_X^{\mathcal{R}}) \text{ with } \ell_{11} \geq 19. \quad (3-7)$$

If X belongs to the perpendicular bisectors of the square, we have more accurately the following:

$$\ell_4 = \ell_4(X) \geq 8, \quad (3-8)$$

$$\lambda_6^{\mathbf{ABX}} \leq \lambda_7(\Omega). \quad (3-9)$$

Remark 3.3. The multiplicity of $\lambda_\ell(\Omega)$ as an eigenvalue of the Dirichlet Laplacian on $\dot{\Omega}_X^{\mathcal{R}}$ is of course greater than or equal to its multiplicity on Ω . This could make it possible to improve some inequalities above when we can find for a given pole, an eigenfunction u of the Dirichlet Laplacian on Ω vanishing at the pole. The number of nodal domains of the lifted symmetric function on the covering is then $2\mu(u)$ instead of $2\mu(u) - 1$, where $\mu(u)$ is the number of

nodal domains of u . To find this eigenfunction could be easier when the eigenspace is of higher dimension. This appears, for example, for $\lambda_2(\Omega)$.

Proof. Let us first prove (3–2). We first observe that for any $X \in [0, \frac{1}{2}] \times [0, \frac{1}{2}]$, there exists an eigenfunction u_X of the Dirichlet Laplacian associated with $\lambda_2(\Omega)$ and $u_X(X) = 0$. We have just to look for u_X of the form $u_X = \alpha\phi_{1,2} + \beta\phi_{2,1}$ with $(\alpha, \beta) \neq (0, 0)$ satisfying $\alpha\phi_{1,2}(X) + \beta\phi_{2,1}(X) = 0$. By lifting on $\dot{\Omega}_X^{\mathcal{R}}$, this gives a $\mathcal{D}_X^{\mathcal{R}}$ -symmetric eigenfunction $u_X \circ \pi_X^{\mathcal{R}}$ for the Dirichlet Laplacian on $\dot{\Omega}_X^{\mathcal{R}}$ associated with $\lambda_2(\Omega)$ and with four nodal domains. Hence by Courant’s theorem, $\lambda_2(\Omega) = \lambda_{\ell_2}(\dot{\Omega}_X^{\mathcal{R}})$ with $\ell_2 \geq 4$. To establish the first inequality in (3–2), we consider the functions $\max(u_X, 0)$ and $\max(-u_X, 0)$, which span a two-dimensional space in the form domain of the \mathbf{ABX} -Hamiltonian for which the energy is less than $\lambda_2(\Omega)$. We can conclude the proof by the minimax principle. It is easy to see that the inequality is strict. Hence at this stage we also get (3–2).

Let us now prove (3–3). Using the three functions obtained by restriction to one nodal domain of the function $\phi_{2,2}$ (then extended by 0) that does not contain X , we obtain a 3-dimensional space of functions in the form domain of the \mathbf{ABX} -Hamiltonian for which the energy is less than $\lambda_4(\Omega)$ (or a 4-dimensional space if X is on the perpendicular bisector of the side of the square because in this case, we can get a 4-dimensional space; see Remark 3.3). We then conclude the proof by the minimax principle. The relation with $\lambda_{\ell_4}(\dot{\Omega}_X^{\mathcal{R}})$ is an application of Courant’s nodal theorem using the function $\phi_{2,2} \circ \pi_X^{\mathcal{R}}$.

Relation (3–4) is a consequence of (3–3). For (3–5), we can use the function $\phi_{3,2}$, which has at least five nodal domains not containing X . For X on the perpendicular bisector, we get (3–9).

The function $\phi_{4,1}$ has at least three nodal domains not containing X . Using (3–5) and the multiplicity of $\lambda_9(\Omega)$, we obtain (3–6). Using the function $\phi_{3,3}$, which has at least eight nodal domains not containing X , we deduce (3–7).

The lower bound for ℓ_7 , ℓ_9 , and ℓ_{11} results immediately from the upper bounds of $\lambda_5^{\mathbf{ABX}}$ by $\lambda_7(\Omega)$ (hence by $\lambda_9(\Omega)$) and of $\lambda_8^{\mathbf{ABX}}$ by $\lambda_{11}(\Omega)$ established in (3–5) and (3–7). \square

Lemma 3.4. *The nodal set of the second K_X -real eigenfunction $u_2^{\mathbf{ABX}}$ consists of one line joining the pole X to the boundary.*

Proof. We know from [Helffer et al. 99] that a piecewise regular line in the nodal set should join the pole X to

the boundary. Another piece in the nodal set should necessarily create an additional nodal domain that will lead to $\lambda_2 \leq \lambda_2^{\mathbf{AB}X}$, in contradiction to (3-2). \square

The inequality $\lambda_1^{\mathbf{AB}X} \geq \lambda_1(\Omega)$ is of course a particular case of the diamagnetic inequality. We will observe in the figures that the situation is much more complicated for excited states. Except in the case of additional symmetries, where some monotonicity will be proven, we have no theoretical results.

Remark 3.5. We will see in Figures 11, 12, and 16 that the upper bounds (3-2), (3-3), and (3-5) in Proposition 3.2 for the $\mathbf{AB}X$ -eigenvalues are optimal in the sense that we can find a pole such that the upper bound is false with a smaller eigenvalue of the square.

4. BEHAVIOR OF THE EIGENVALUES ON THE DOUBLE COVERING OF THE PUNCTURED SQUARE WHEN MOVING THE POLE

In this section, we begin to discuss the influence of the location of the puncturing point X (or pole) on the topological structure of the nodal set of the first eigenfunctions.

4.1. Behavior When the Pole Tends to the Boundary

It was announced in [Noris and Terracini 10] that the k th $\mathbf{AB}X$ -eigenvalue of the punctured square tends to the k th eigenvalue of the Dirichlet Laplacian on the square as the pole tends to the boundary (see also [Hillairet and Judge 10] for related results). Also established in [Noris and Terracini 10] is the continuity with respect to a pole, and the authors prove that $X \mapsto \lambda_k^{\mathbf{AB}X}$ is of class C^1 if $\lambda_k^{\mathbf{AB}X}$ is simple.

Because after a translation by X , we get a fixed operator with moving regular boundary and fixed pole at $(0, 0)$, the regularity is actually easy. These results are illustrated in Figures 3 through 7, which represent the eigenvalues $\lambda_k(\dot{\Omega}_X^{\mathcal{R}})$, $k = 2, 3, 6, 7$, according to the location of the pole $X \in \mathcal{P}$, and Table 2, which gives the first 12 eigenvalues of the Dirichlet Laplacian on $\dot{\Omega}_X^{\mathcal{R}}$ for three points X : one near the boundary, denoted by A ; one at the center, denoted by C ; and one other, denoted by B .

4.2. Eigenvalues 2 to 5

We observe numerically, see Figure 3, that for $X \in \mathcal{P}$, the function $X \mapsto \lambda_2(\dot{\Omega}_X^{\mathcal{R}})$ has a global maximum, denoted by λ_2^{\max} for $X = C$, and is minimal when X belongs to the boundary $x = 0$ or $y = 0$. This minimum

equals $\lambda_2(\Omega)$. Moreover, we do not observe other critical points in \mathcal{P} . Looking at Figure 4, we observe numerically that the function $X \mapsto \lambda_3(\dot{\Omega}_X^{\mathcal{R}})$ behaves conversely: it has a global minimum, denoted by λ_3^{\min} , for $X = C$, and the maximum is reached at the boundary $x = 0$ or $y = 0$ and equals $\lambda_3(\Omega)$. We have monotonicity along lines joining a point of the boundary to the center C . Furthermore, we notice that $\lambda_2^{\max} = \lambda_3^{\min}$.

Figure 5 gives the eigenvalues and the nodal lines of the eigenfunctions associated with the second and third eigenvalues of the Dirichlet Laplacian on $\dot{\Omega}_X^{\mathcal{R}}$ on the first and second lines respectively. The j th column corresponds to the domain $\dot{\Omega}_{X_j}^{\mathcal{R}}$ with $X_j = (\frac{1}{5}, \frac{j}{10})$, $j = 1, \dots, 5$. These figures are an illustration of the theory of [Berger and Rubinstein 99] and [Helffer et al. 99]; see also [Alziary et al. 03].

For the ground-state energy, we recover the theorem of these authors that the nodal set is composed of a line joining the pole to the boundary. We observe that the nodal line in the first case is choosing a kind of minimal distance between the pole and the boundary, whereas the nodal line in the second case seems to choose a kind of maximal distance. We do not have a rigorous explanation for this property except that it should be related to the theorem proved in [Berger and Rubinstein 99, Helffer et al. 99] that $\lambda_1^{\mathbf{AB}X}$ is the infimum over the Dirichlet eigenvalue of the Laplacian in $\Omega \setminus \gamma$, where γ is a regular path joining the pole X to the boundary. We also recover the two last equations in (3-1).

Using (3-2), we have proved that $\lambda_2(\Omega) \geq \lambda_5(\dot{\Omega}_X^{\mathcal{R}})$. We observe numerically (see also Figures 11 and 12 for poles along a symmetry axis and Figure 16) that for any $X \in \mathcal{P}$, we have

$$\lambda_4(\dot{\Omega}_X^{\mathcal{R}}) = \lambda_5(\dot{\Omega}_X^{\mathcal{R}}) = \lambda_2(\Omega). \tag{4-1}$$

4.3. Eigenvalues 6 and 7

Computations show that the sixth eigenvalue $\lambda_6(\dot{\Omega}_X^{\mathcal{R}})$ is minimal at the boundary and has a unique maximum $\lambda_6^{\max} \approx 66.581$, attained for the pole at the center. We do not observe other critical points. The seventh eigenvalue $\lambda_7(\dot{\Omega}_X^{\mathcal{R}})$ is minimal when the pole is at the center, and its minimum λ_7^{\min} is equal to λ_6^{\max} . When the pole is at the center, the zero set of the sixth eigenfunction provides, by projection, a candidate for a 3-partition, and λ_6^{\max} is the conjectured value for $\mathfrak{L}_3(\Omega)$.

We observe that the seventh eigenvalue becomes constant, equal to $\lambda_7^{\max} = \lambda_4(\Omega) = 8\pi^2$, as a function of the pole when the pole is close to the boundary.

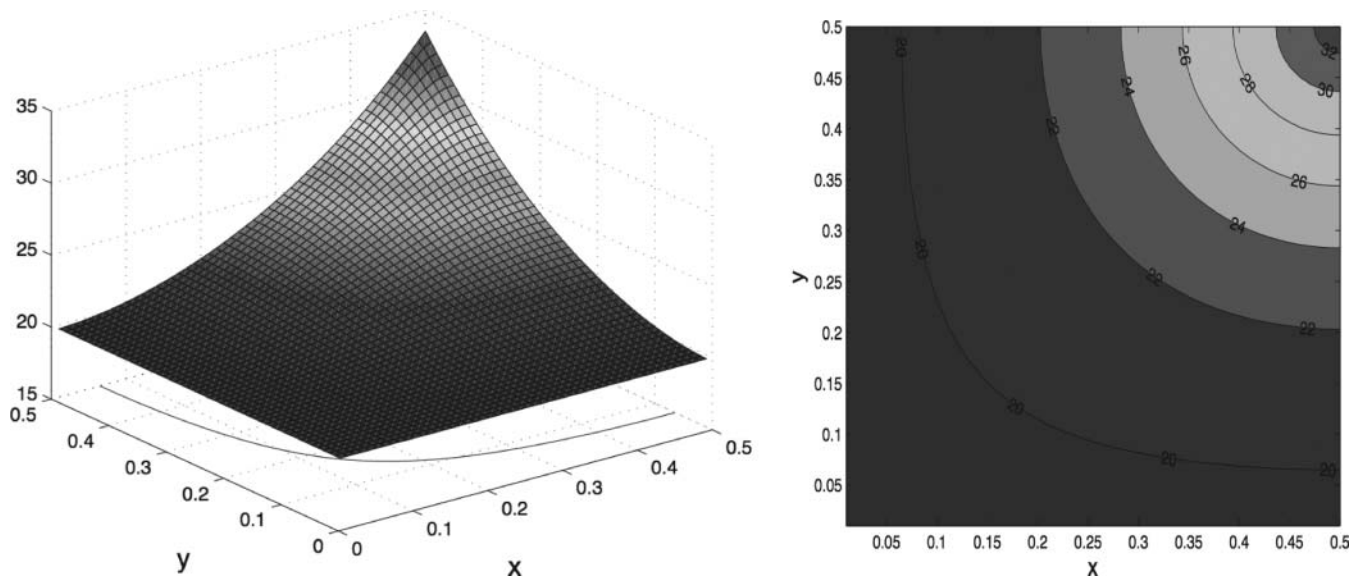


FIGURE 3. $X \mapsto \lambda_2(\hat{\Omega}_X^R)$ for $X \in \mathcal{P}$.

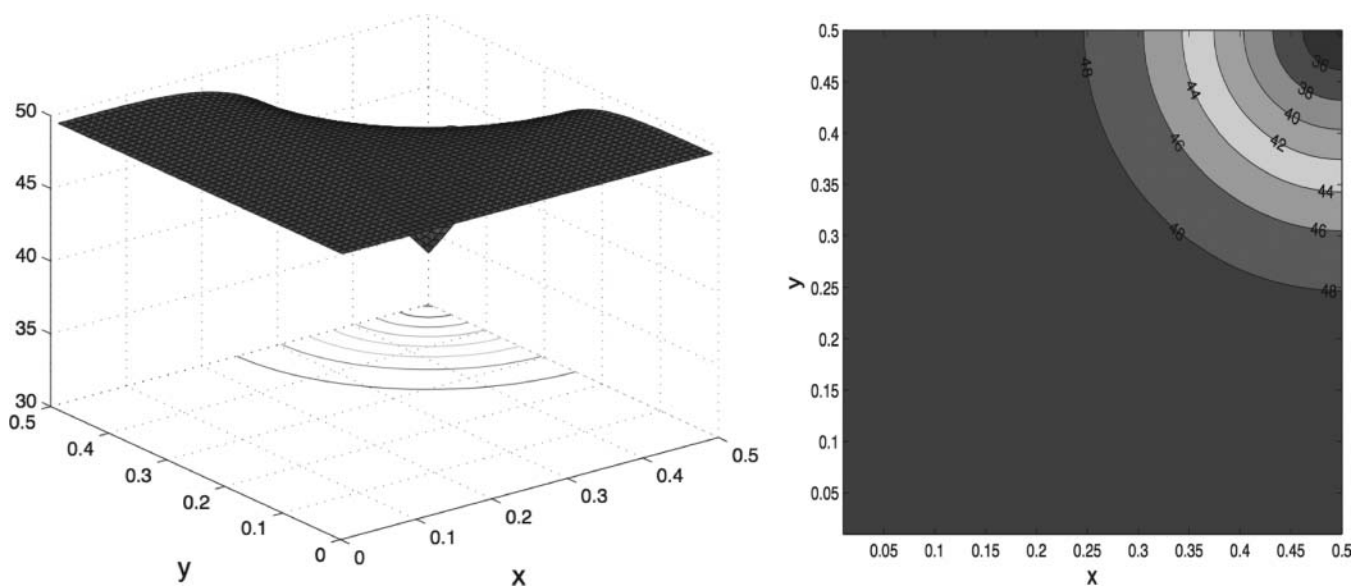


FIGURE 4. $X \mapsto \lambda_3(\hat{\Omega}_X^R)$ for $X \in \mathcal{P}$.

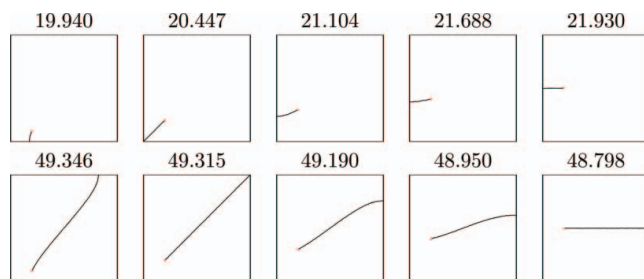


FIGURE 5. Nodal set for the eigenfunctions associated with $\lambda_k(\hat{\Omega}_X^R)$, $k = 2, 3$, for poles $X = (\frac{1}{5}, \frac{j}{10})$, $1 \leq j \leq 5$ (color figure available online).

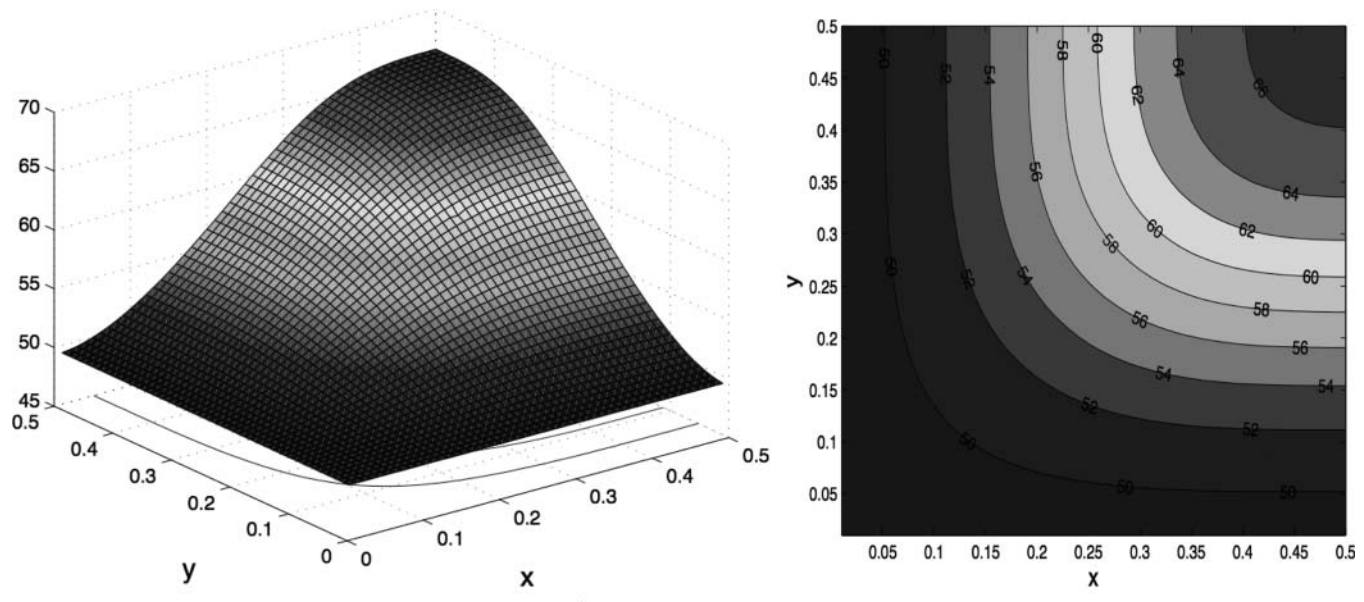


FIGURE 6. $\lambda_6(\dot{\Omega}_X^R)$, as a function of the pole $X \in \mathcal{P}$.

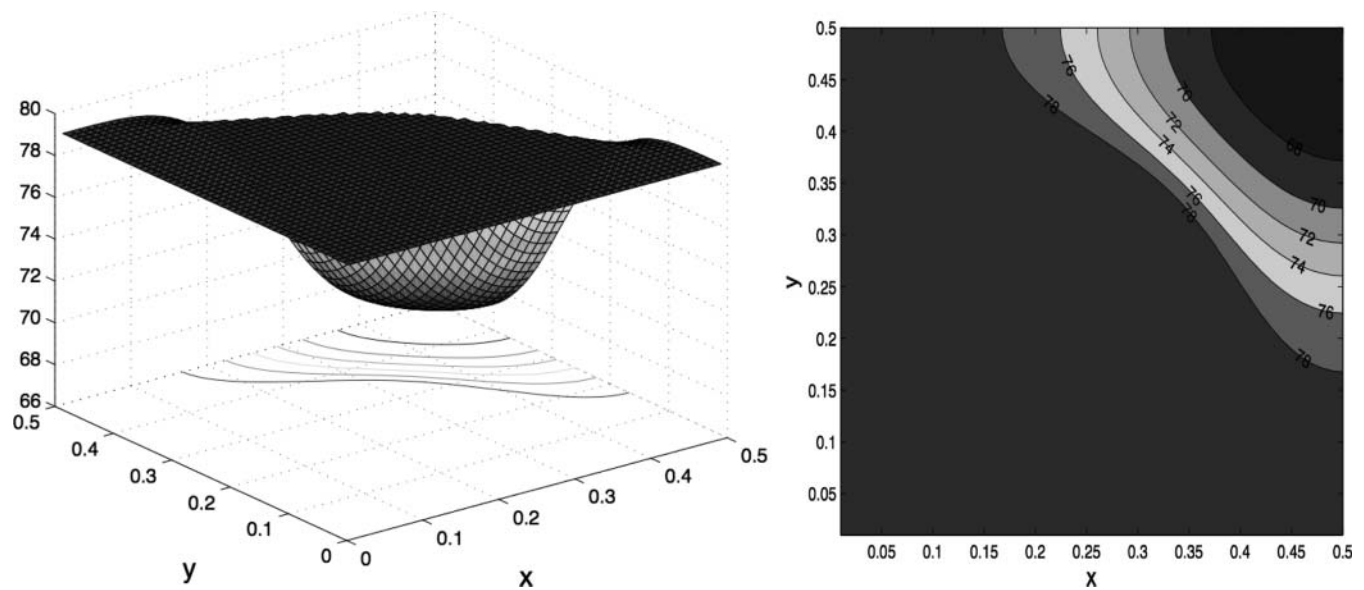


FIGURE 7. $\lambda_7(\dot{\Omega}_X^R)$, as a function of the pole $X \in \mathcal{P}$.

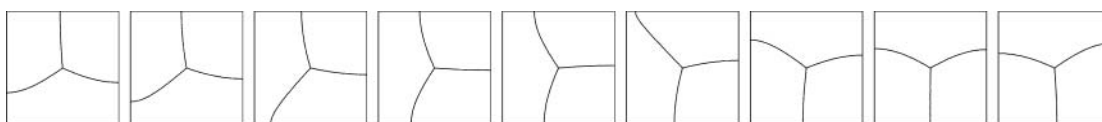


FIGURE 8. Continuous family of 3-partitions with the same energy.

n	$\lambda_n(\dot{\Omega}_A^{\mathcal{R}})$	$\lambda_n(\dot{\Omega}_B^{\mathcal{R}})$	$\lambda_n(\dot{\Omega}_C^{\mathcal{R}})$
1	19.739	19.739	19.739
2	19.739	20.269	33.528
3	49.348	49.325	33.534
4	49.348	49.348	49.348
5	49.348	49.348	49.348
6	49.348	51.480	66.581
7	78.957	78.957	66.581
8	78.957	79.536	78.957
9	98.696	98.658	98.696
10	98.696	98.696	98.696
11	98.696	98.696	111.910
12	98.696	102.647	111.910

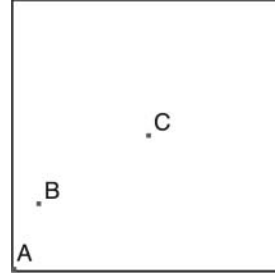


TABLE 2. First 12 eigenvalues of the Dirichlet Laplacian on $\dot{\Omega}_A^{\mathcal{R}}$, $\dot{\Omega}_B^{\mathcal{R}}$, and $\dot{\Omega}_C^{\mathcal{R}}$, with $A = (\frac{1}{100}, \frac{1}{100})$, $B = (\frac{1}{10}, \frac{2}{5})$, $C = (\frac{1}{2}, \frac{1}{2})$.

This corresponds to a crossing when X approaches the boundary between the spectrum of the square (i.e., the $\mathcal{D}_X^{\mathcal{R}}$ -symmetric spectrum on the covering) and the X -dependent **ABX**-spectrum (i.e., the $\mathcal{D}_X^{\mathcal{R}}$ -antisymmetric spectrum on the covering $\dot{\Omega}_X^{\mathcal{R}}$).

Applying relation (3–3), we have proved theoretically that $\lambda_4(\Omega) \geq \lambda_7(\dot{\Omega}_X^{\mathcal{R}})$. We observe numerically that this relation is optimal in the sense that we have equality for X close to the boundary.

Considering the linear combination of the eigenfunctions u_6 and u_7 associated respectively with $\lambda_6(\dot{\Omega}_C^{\mathcal{R}})$ and $\lambda_7(\dot{\Omega}_C^{\mathcal{R}})$, with $C = (\frac{1}{2}, \frac{1}{2})$, we can construct a family of 3-partitions with the same energy. Figure 8 gives the projection by $\pi_C^{\mathcal{R}}$ of the nodal set for the functions $tu_6 + (1-t)u_7$ with $t = \frac{k}{8}$, $k = 0, \dots, 8$.

It is interesting to consider whether we can prove the numerically observed inequality

$$\lambda_3^{\mathbf{ABX}} \geq \lambda_2(\Omega). \quad (4-2)$$

This is directly related to a conjecture proposed by S. Terracini:³

Conjecture 4.1. *Except at the center $X = C = (\frac{1}{2}, \frac{1}{2})$, $\lambda_3^{\mathbf{ABX}}$ is simple, and the corresponding nodal set of the K_X -real eigenfunction is the union of a line joining the pole to the boundary and of another line joining two points of the boundary.*

We note that if the conjecture is true, we will get (4–2) by the minimax principle.

4.4. Eigenvalues 8 to 10

Figures 9 and 10 represent the numerical computations of $\lambda_8(\dot{\Omega}_X^{\mathcal{R}})$ and $\lambda_9(\dot{\Omega}_X^{\mathcal{R}})$ for $X \in \mathcal{P}$. We observe numerically that the function $X \mapsto \lambda_8(\dot{\Omega}_X^{\mathcal{R}})$ has a unique maximum denoted by λ_8^{\max} at a point C_1 on the diagonal and $X \mapsto \lambda_9(\dot{\Omega}_X^{\mathcal{R}})$ reaches its unique minimum, λ_9^{\min} , at this point. We can recover this behavior in Figure 11, where are drawn the eigenvalues for poles on the diagonal. Numerically, $\lambda_8^{\max} = \lambda_9^{\min}$ and we return to this equality in Section 5, where we look at the nodal lines of the eigenfunctions associated with $\lambda_8(\dot{\Omega}_X^{\mathcal{R}})$ and $\lambda_9(\dot{\Omega}_X^{\mathcal{R}})$ and predict the existence of the point C_1 ; see Figure 14(a).

According to (3–8), we have proved that $\lambda_8(\dot{\Omega}_X^{\mathcal{R}}) \leq \lambda_7(\Omega)$. This theoretical upper bound is rough, and the numerics suggest that we have in fact the better bound $\lambda_8(\dot{\Omega}_X^{\mathcal{R}}) \leq \lambda_5(\Omega)$. Moreover, C_1 is singular for the maps $X \mapsto \lambda_8(\dot{\Omega}_X^{\mathcal{R}})$ and $\lambda_9(\dot{\Omega}_X^{\mathcal{R}})$.

We observe numerically that for any $X \in \mathcal{P}$, we have

$$\lambda_{10}(\dot{\Omega}_X^{\mathcal{R}}) = \lambda_5(\Omega).$$

What we have proven in (3–4) is weaker.

5. MOVING THE POLE ALONG THE SYMMETRY AXIS

5.1. Analysis of the Symmetries

Let us begin with some considerations about the **ABX**-Hamiltonian on the X -punctured square, using the symmetry along the perpendicular bisector $y = \frac{1}{2}$ or the

³Personal communication.

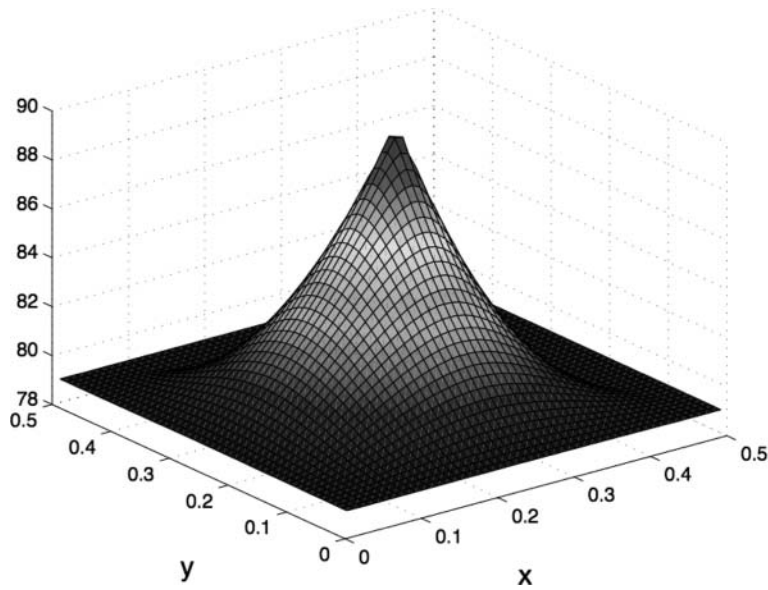


FIGURE 9. $X \mapsto \lambda_8(\dot{\Omega}_X^R)$ for $X \in \mathcal{P}$.

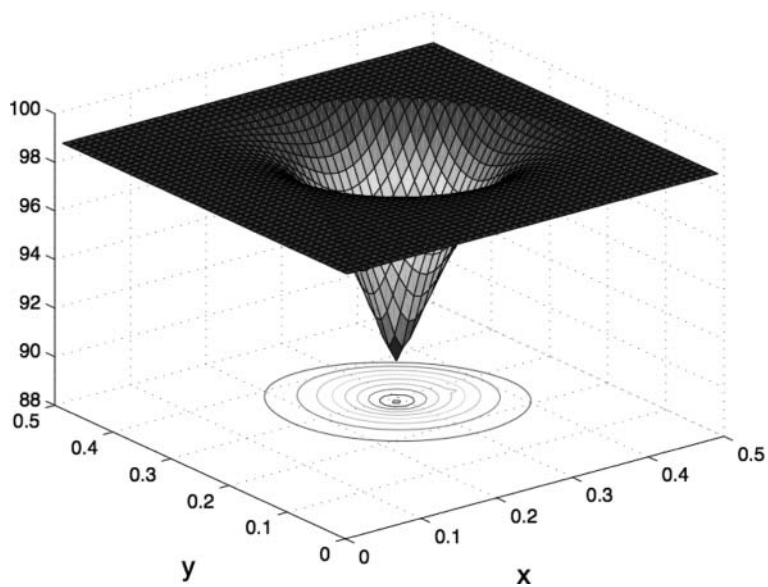
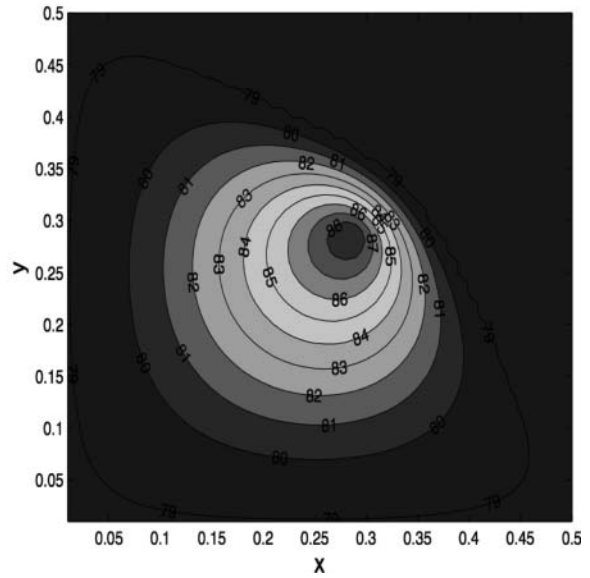
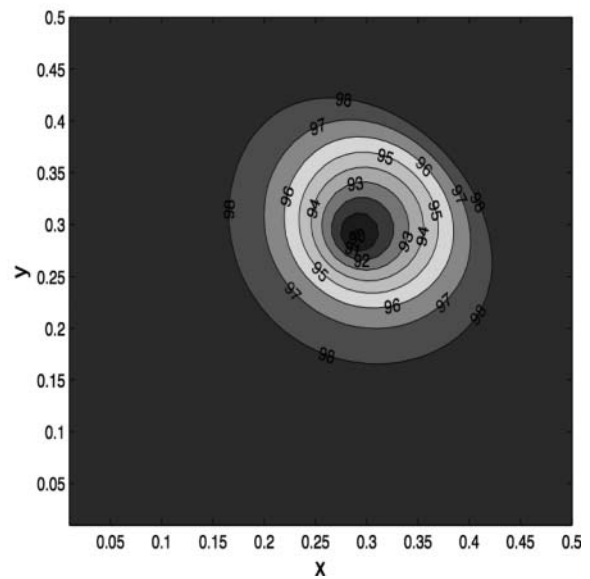


FIGURE 10. $X \mapsto \lambda_9(\dot{\Omega}_X^R)$ for $X \in \mathcal{P}$.



diagonal $y = x$. We refer to [Bonnaillie-Noël et al. 09] for more details. The square is invariant under the symmetries

$$\sigma_1(x, y) = (x, 1 - y) \quad \text{and} \quad \sigma_2(x, y) = (y, x).$$

We consider the antilinear operators

$$\Sigma_j^c = \Gamma \Sigma_j, \quad j = 1, 2,$$

where Γ is the complex conjugation ($\Gamma u = \bar{u}$) and Σ_j is associated with σ_j by the relations $\Sigma_1 u(x, y) = u(x, 1 - y)$ and $\Sigma_2 u(x, y) = u(y, x)$.

We use the symmetry of the X -punctured square to give an orthogonal decomposition of $L_K^2 = L_{K_X}^2$:

$$L_K^2 = L_{K, \Sigma_j}^2 \oplus L_{K, a \Sigma_j}^2,$$

where

$$\begin{aligned} L_{K, \Sigma_j}^2 &= \{u \in L_K^2 \mid \Sigma_j^c u = u\}, \\ L_{K, a \Sigma_j}^2 &= \{u \in L_K^2 \mid \Sigma_j^c u = -u\}. \end{aligned} \tag{5-1}$$

As established in [Bonnaillie-Noël et al. 09, Lemma 5.6], we can prove that:

if $X = (x_0, \frac{1}{2})$:

- if $u \in C^\infty(\dot{\Omega}_X) \cap L^2_{K, \Sigma_1}$, then its nodal set contains $[0, x_0] \times \{\frac{1}{2}\}$,
- if $u \in C^\infty(\dot{\Omega}_X) \cap L^2_{K, a\Sigma_1}$, then its nodal set contains $[x_0, 1] \times \{\frac{1}{2}\}$,

if $X = (x_0, x_0)$:

- if $u \in C^\infty(\dot{\Omega}_X) \cap L^2_{K, \Sigma_2}$, then the nodal set of u contains $\{(x, x), 0 < x < x_0\}$,
- if $u \in C^\infty(\dot{\Omega}_X) \cap L^2_{K, a\Sigma_2}$, then the nodal set of u contains $\{(x, x), x_0 < x < 1\}$.

Dealing with a mixed Dirichlet–Neumann condition on the half-domain, we deduce that the eigenvalues for which the eigenfunctions are symmetric are increasing with respect to x_0 , whereas the eigenvalues for which the eigenfunctions are antisymmetric are decreasing with respect to x_0 .

5.2. Spectral Variation

Figures 11 and 12 give the eigenvalues for poles along the axes $y = \frac{1}{2}$ and $y = x$ respectively and $0 < x \leq \frac{1}{2}$. Poles are denoted by $X(x) = (x, \frac{1}{2})$ and $\check{X}(x) = (x, x)$. The below-mentioned symmetry (respectively antisymmetry) is in this section with respect to Σ_j^c (see (5–1)) and denoted by Σ_j (respectively $a\Sigma_j$) in the figures, where $j = 1$ when we consider poles $X(x)$ and $j = 2$ for poles $\check{X}(x)$.

Let us first mention some numerical observations available for these two configurations:

1. $\lim_{x \rightarrow 0} \lambda_k^{\mathbf{AB}X(x)} = \lambda_k(\Omega)$ and $\lim_{x \rightarrow 0} \lambda_k^{\mathbf{AB}\check{X}(x)} = \lambda_k(\Omega)$.
2. For any integer $0 \leq k \leq 3$, $\lambda_{2k+1}^{\mathbf{ABC}} = \lambda_{2k+2}^{\mathbf{ABC}}$.
3. $x \mapsto \lambda_1(\dot{\Omega}_{X(x)}^{\mathcal{R}})$ and $x \mapsto \lambda_1(\dot{\Omega}_{\check{X}(x)}^{\mathcal{R}})$ equal $\lambda_1(\Omega)$, in accord with the theoretical result (3–1).
4. $x \mapsto \lambda_2(\dot{\Omega}_{X(x)}^{\mathcal{R}}) = \lambda_1^{\mathbf{AB}X(x)}$ and $x \mapsto \lambda_2(\dot{\Omega}_{\check{X}(x)}^{\mathcal{R}}) = \lambda_1^{\mathbf{AB}\check{X}(x)}$ are strictly increasing from $[0, \frac{1}{2}]$ onto $[\lambda_1(\Omega), \lambda_1^{\mathbf{ABC}}]$ and the eigenfunctions are symmetric. The equality between $\lambda_2(\dot{\Omega}_{X(x)}^{\mathcal{R}})$ and $\lambda_1^{\mathbf{AB}X}$ was proved in (3–1).
5. $x \mapsto \lambda_3(\dot{\Omega}_{X(x)}^{\mathcal{R}}) = \lambda_2^{\mathbf{AB}X(x)}$ and $x \mapsto \lambda_3(\dot{\Omega}_{\check{X}(x)}^{\mathcal{R}}) = \lambda_2^{\mathbf{AB}\check{X}(x)}$ are strictly decreasing from $[0, \frac{1}{2}]$ onto $[\lambda_2^{\mathbf{ABC}}, \lambda_2(\Omega)]$ and the eigenfunctions are antisymmetric. The equality between $\lambda_3(\dot{\Omega}_{X(x)}^{\mathcal{R}})$ and $\lambda_2^{\mathbf{AB}X}$ was proved in (3–1).

6. $\lambda_4(\dot{\Omega}_{X(x)}^{\mathcal{R}}) = \lambda_5(\dot{\Omega}_{\check{X}(x)}^{\mathcal{R}}) = \lambda_2(\Omega)$, for $X = X(x)$ or $X = \check{X}(x)$. This numerical observation is more accurate than the theoretical result deduced from (3–2): $\lambda_4(\dot{\Omega}_{X(x)}^{\mathcal{R}}) \leq \lambda_2(\Omega)$. This relation seems to be an equality for any X ; see Section 4.2.

7. $x \mapsto \lambda_6(\dot{\Omega}_{X(x)}^{\mathcal{R}}) = \lambda_3^{\mathbf{AB}X(x)}$ and $x \mapsto \lambda_6(\dot{\Omega}_{\check{X}(x)}^{\mathcal{R}}) = \lambda_3^{\mathbf{AB}\check{X}(x)}$ are strictly increasing from $[0, \frac{1}{2}]$ onto $[\lambda_3(\Omega), \lambda_3^{\mathbf{ABC}}]$ and the eigenfunctions are symmetric.

Once the symmetry is admitted, the monotonicity results directly in a domain monotonicity.

Let us now discuss properties specific to each symmetry.

Spectral variation for poles along the axis $y = \frac{1}{2}$. We observe that when $X(x) = (x, \frac{1}{2})$, $x \mapsto \lambda_k^{\mathbf{AB}X(x)}$ is monotonically increasing for $k = 1, 3, 5$, whereas it is decreasing for $k = 2, 4$.

We introduce $A_j = X(a_j)$, $B_j = X(b_j)$, specific points that can be seen in Figure 11. We observe the following numerically:

- (8_a) $x \mapsto \lambda_7(\dot{\Omega}_{X(x)}^{\mathcal{R}}) = \lambda_4^{\mathbf{AB}X(x)}$ is strictly decreasing from $[0, \frac{1}{2}]$ onto $[\lambda_4^{\mathbf{ABC}}, \lambda_4(\Omega)]$ and the eigenfunctions are antisymmetric.

- (9_a) $\lambda_8(\dot{\Omega}_{X(x)}^{\mathcal{R}}) = \lambda_4(\Omega)$. We have proved in (3–8) that $\lambda_8(\dot{\Omega}_{X(x)}^{\mathcal{R}}) \leq \lambda_4(\Omega)$ and we observe that this upper bound is actually an equality. We notice that there is a gap between $\lambda_4(\Omega)$ and $\lambda_5(\Omega)$, where there is no eigenvalue $\lambda_k(\dot{\Omega}_{X(x)}^{\mathcal{R}})$ for X on the perpendicular bisector. This observation is no longer true for poles on the diagonal (see Figure 12).

- (10_a) $\lambda_9(\dot{\Omega}_{X(x)}^{\mathcal{R}}) = \lambda_{10}(\dot{\Omega}_{X(x)}^{\mathcal{R}}) = \lambda_5(\Omega)$.

- (11_a) $x \mapsto \lambda_{11}(\dot{\Omega}_{X(x)}^{\mathcal{R}}) = \lambda_5^{\mathbf{AB}X(x)}$ is strictly increasing from $[0, \frac{1}{2}]$ onto $[\lambda_5(\Omega), \lambda_5^{\mathbf{ABC}}]$ and the eigenfunctions are symmetric. This observation shows that the theoretical upper bound $\lambda_{11}(\dot{\Omega}_{X(x)}^{\mathcal{R}}) \leq \lambda_7(\Omega)$ deduced from (3–5) cannot be improved.

- (12_a) $x \mapsto \lambda_{12}(\dot{\Omega}_{X(x)}^{\mathcal{R}}) = \lambda_6^{\mathbf{AB}X(x)}$ is strictly increasing from $[0, a_1]$ onto $[\lambda_6(\Omega), \lambda_6^{\mathbf{ABA}_1}]$ and the eigenfunctions are symmetric. It is strictly decreasing from $[a_1, \frac{1}{2}]$ onto $[\lambda_6^{\mathbf{ABC}}, \lambda_6^{\mathbf{ABA}_1}]$, and the eigenfunctions are antisymmetric. This illustrates a theoretical result deduced from (3–9), $\lambda_{12}(\dot{\Omega}_{X(x)}^{\mathcal{R}}) \leq \lambda_7(\Omega)$, and shows that this result is optimal.

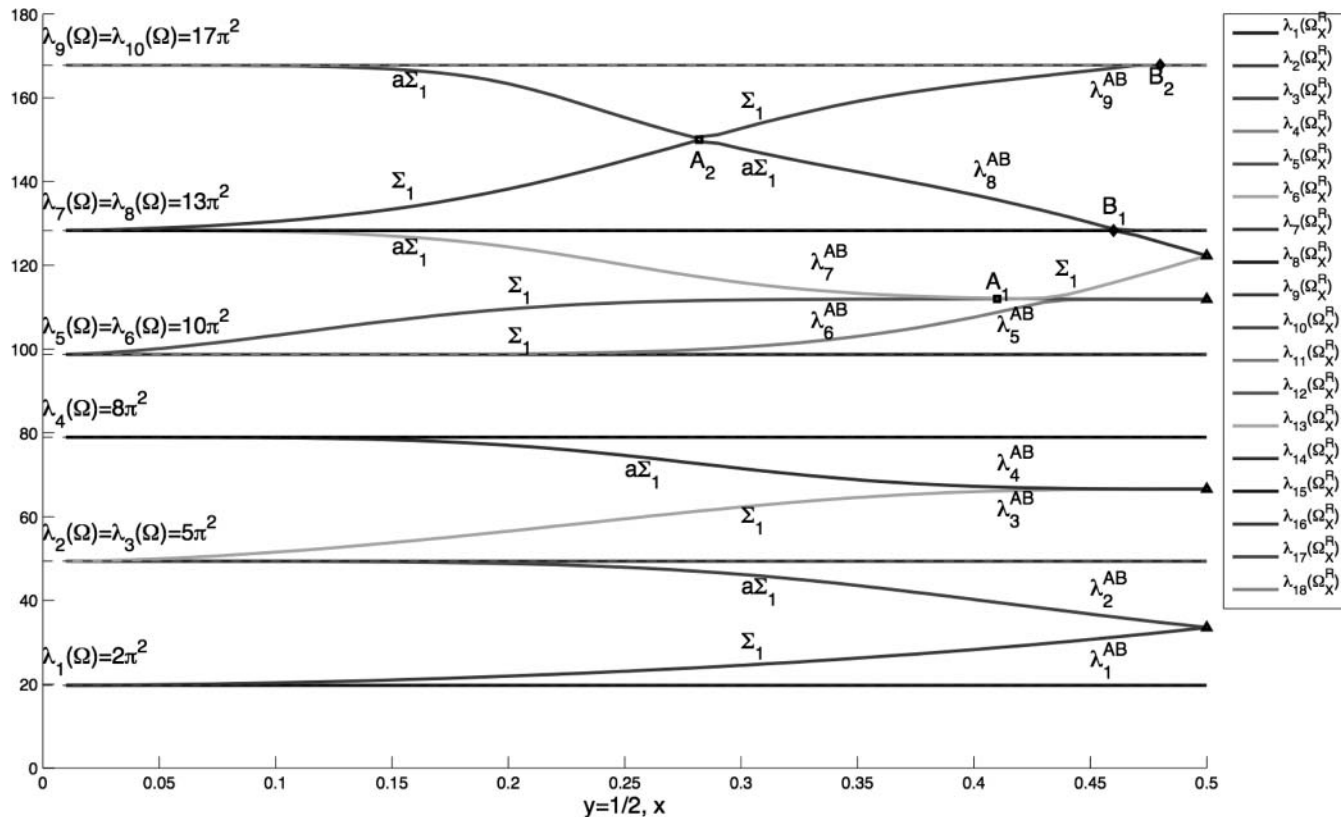


FIGURE 11. Moving the pole along the axis $y = \frac{1}{2}$.

(13a) $x \mapsto \lambda_{13}(\dot{\Omega}_{\check{X}}^{\mathcal{R}}(x)) = \lambda_7^{\mathbf{AB}\check{X}}(x)$ is strictly decreasing from $[0, a_1]$ onto $[\lambda_7(\Omega), \lambda_7^{\mathbf{AB}A_1}]$, and the eigenfunctions are antisymmetric. It is strictly increasing from $[a_1, \frac{1}{2}]$ onto $[\lambda_7^{\mathbf{ABC}}, \lambda_7^{\mathbf{AB}A_1}]$, and the eigenfunctions are symmetric. We observe then that $\lambda_{13}(\dot{\Omega}_{\check{X}}^{\mathcal{R}})$ can be bounded from above by $\lambda_7(\Omega)$, whereas we have proved in (3–6) the upper bound by $\lambda_9(\Omega)$.

(14a) $\lambda_{14}(\dot{\Omega}_{\check{X}}^{\mathcal{R}}(x))$ equals $\lambda_8(\Omega)$ on $[0, b_1]$. It equals $\lambda_8^{\mathbf{AB}\check{X}}(x)$ on $[b_1, \frac{1}{2}]$ and is strictly decreasing from $[b_1, \frac{1}{2}]$ onto $[\lambda_8^{\mathbf{ABC}}, \lambda_8(\Omega)]$ with antisymmetric eigenfunctions.

(15a) $\lambda_{15}(\dot{\Omega}_{\check{X}}^{\mathcal{R}}(x)) = \lambda_8(\Omega)$.

Spectral variation for poles along the axis $y = x$. Figure 12 gives the eigenvalues for poles along the diagonal line of the square $x = y$ with $0 < x \leq \frac{1}{2}$.

We introduce $C_j = \check{X}(c_j)$, $D_j = \check{X}(d_j)$, specific crossing points appearing in the figure. Then, we observe the following:

(8b) $x \mapsto \lambda_7(\dot{\Omega}_{\check{X}}^{\mathcal{R}}(x))$ equals $\lambda_4(\Omega)$ on $[0, d_1]$ and $\lambda_4^{\mathbf{AB}\check{X}}(x)$ on $[d_1, \frac{1}{2}]$, where it is strictly decreasing onto $[\lambda_4^{\mathbf{ABC}}, \lambda_4(\Omega)]$ and the eigenfunctions are antisymmetric. These numerical computations show that the theoretical estimate $\lambda_7(\dot{\Omega}_{\check{X}}^{\mathcal{R}}) \leq \lambda_4(\Omega)$ deduced from (3–3) is optimal.

(9b) $\lambda_8(\dot{\Omega}_{\check{X}}^{\mathcal{R}}(x))$ equals $\lambda_4^{\mathbf{AB}\check{X}}(x)$ on $[0, d_1]$ and $\lambda_4(\Omega)$ on $[d_1, \frac{1}{2}]$. It is strictly increasing from $[0, c_1]$ onto $[\lambda_4(\Omega), \lambda_4(\dot{\Omega}_{C_1}^{\mathcal{R}})]$ with symmetric eigenfunctions and strictly decreasing from $[c_1, d_1]$ onto $[\lambda_4(\Omega), \lambda_4(\dot{\Omega}_{C_1}^{\mathcal{R}})]$ with antisymmetric eigenfunctions. This illustrates that (3–4) is optimal.

(10b) $\lambda_9(\dot{\Omega}_{\check{X}}^{\mathcal{R}}(x))$ equals $\lambda_5^{\mathbf{AB}\check{X}}(x)$ on $[0, d_2]$ and $\lambda_5(\Omega)$ on $[d_2, \frac{1}{2}]$. It is strictly decreasing from $[0, c_1]$ onto $[\lambda_4(\dot{\Omega}_{C_1}^{\mathcal{R}}), \lambda_5(\Omega)]$ with antisymmetric eigenfunctions and strictly increasing from $[c_1, d_1]$ onto $[\lambda_4(\dot{\Omega}_{C_1}^{\mathcal{R}}), \lambda_5(\Omega)]$ with symmetric eigenfunctions.

(11b) $\lambda_{10}(\dot{\Omega}_{\check{X}}^{\mathcal{R}}(x)) = \lambda_5(\Omega)$.

(12b) $x \mapsto \lambda_{11}(\dot{\Omega}_{\check{X}}^{\mathcal{R}}(x))$ equals $\lambda_5(\Omega)$ on $[0, d_2]$ and $\lambda_5^{\mathbf{AB}\check{X}}(x)$ on $[d_2, \frac{1}{2}]$, where it is strictly increasing

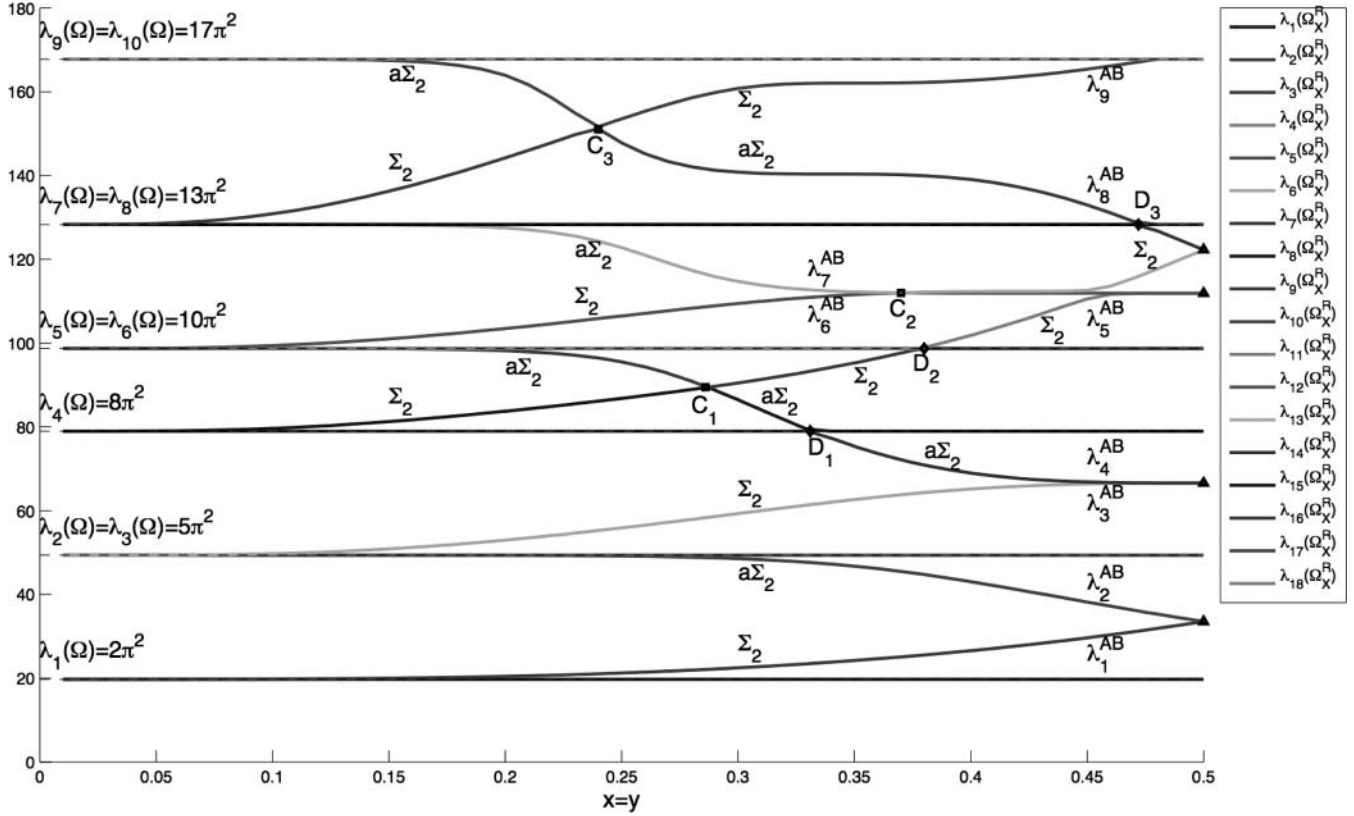


FIGURE 12. Moving the poles on the diagonal.

onto $[\lambda_5(\Omega), \lambda_5^{\text{ABC}}]$ and the eigenfunctions are symmetric. This illustrates the fact that relation (3–5) is optimal.

(13_b) $x \mapsto \lambda_{12}(\dot{\Omega}_{\tilde{X}(x)}^{\mathcal{R}}) = \lambda_6^{\text{AB}\tilde{X}(x)}$ is strictly increasing from $[0, c_2]$ onto $[\lambda_6(\Omega), \lambda_6^{\text{ABC}_2}]$ and the eigenfunctions are symmetric. It is strictly decreasing from $[c_2, \frac{1}{2}]$ onto $[\lambda_6^{\text{ABC}}, \lambda_6^{\text{ABC}_2}]$ and the eigenfunctions are antisymmetric.

(14_b) $x \mapsto \lambda_{13}(\dot{\Omega}_{\tilde{X}(x)}^{\mathcal{R}}) = \lambda_7^{\text{AB}\tilde{X}(x)}$ is strictly decreasing from $[0, c_2]$ onto $[\lambda_7(\Omega), \lambda_7^{\text{ABC}_2}]$ and the eigenfunctions are antisymmetric. It is strictly increasing from $[c_2, \frac{1}{2}]$ onto $[\lambda_7^{\text{ABC}}, \lambda_7^{\text{ABC}_2}]$ and the eigenfunctions are symmetric. We then observe $\lambda_{13}(\dot{\Omega}_{\tilde{X}(x)}^{\mathcal{R}}) \leq \lambda_7(\Omega)$, whereas we have proved the weaker upper bound by $\lambda_9(\Omega)$ in (3–6).

(15_b) $\lambda_{14}(\dot{\Omega}_{\tilde{X}(x)}^{\mathcal{R}})$ equals $\lambda_7(\Omega)$ on $[0, d_3]$. It equals $\lambda_8^{\text{AB}\tilde{X}(x)}$ on $[d_3, \frac{1}{2}]$ and is strictly decreasing from $[d_3, \frac{1}{2}]$ onto $[\lambda_8^{\text{ABC}}, \lambda_8(\Omega)]$ with antisymmetric eigenfunctions.

(16_b) $\lambda_{15}(\dot{\Omega}_{\tilde{X}(x)}^{\mathcal{R}}) = \lambda_8(\Omega)$.

5.3. Exchange of Symmetry and Crossing Points

In moving the pole on one bisector or one diagonal, and for each eigenvalue of multiplicity 1, the corresponding K_X -real eigenfunction should be either symmetric or antisymmetric with respect to Σ_j^c . Figure 11 suggests that there exist two poles $A_1 = (a_1, \frac{1}{2})$ and $A_2 = (a_2, \frac{1}{2})$ on the perpendicular bisector such that $\lambda_{12}(\dot{\Omega}_{A_1}^{\mathcal{R}})$ and $\lambda_{16}(\dot{\Omega}_{A_2}^{\mathcal{R}})$ are eigenvalues of multiplicity 2. Taking the Aharonov–Bohm point of view, this corresponds to a crossing between $\lambda_6^{\text{AB}\tilde{X}(x)}$ and $\lambda_7^{\text{AB}\tilde{X}(x)}$ for $x = a_1$, with $a_1 \in]\frac{42}{100}, \frac{43}{100}[$, and to a crossing between $\lambda_8^{\text{AB}\tilde{X}(x)}$ and $\lambda_9^{\text{AB}\tilde{X}(x)}$ at $x = a_2$, with $a_2 \in]\frac{28}{100}, \frac{29}{100}[$. The nodal sets of the corresponding eigenfunctions are given in Figure 13. The first line gives the eigenvalues $\lambda_6^{\text{AB}\tilde{X}(x)}$, $\lambda_8^{\text{AB}\tilde{X}(x)}$ and the associated nodal sets, and the second line $\lambda_7^{\text{AB}\tilde{X}(x)}$, $\lambda_9^{\text{AB}\tilde{X}(x)}$ and the corresponding nodal set for X along the perpendicular bisector and close to A_1, A_2 .

Figure 12 suggests that there are three points, C_1, C_2 , and C_3 , on the diagonal such that $\lambda_8(\dot{\Omega}_{C_1}^{\mathcal{R}})$, $\lambda_{12}(\dot{\Omega}_{C_2}^{\mathcal{R}})$, and $\lambda_{16}(\dot{\Omega}_{C_3}^{\mathcal{R}})$ are eigenvalues of multiplicity 2. This corresponds to a crossing between $\lambda_4^{\text{AB}\tilde{X}(x)}$ and $\lambda_5^{\text{AB}\tilde{X}(x)}$ at $x = c_1$, with $c_1 \in]\frac{28}{100}, \frac{29}{100}[$. Similarly, there is a

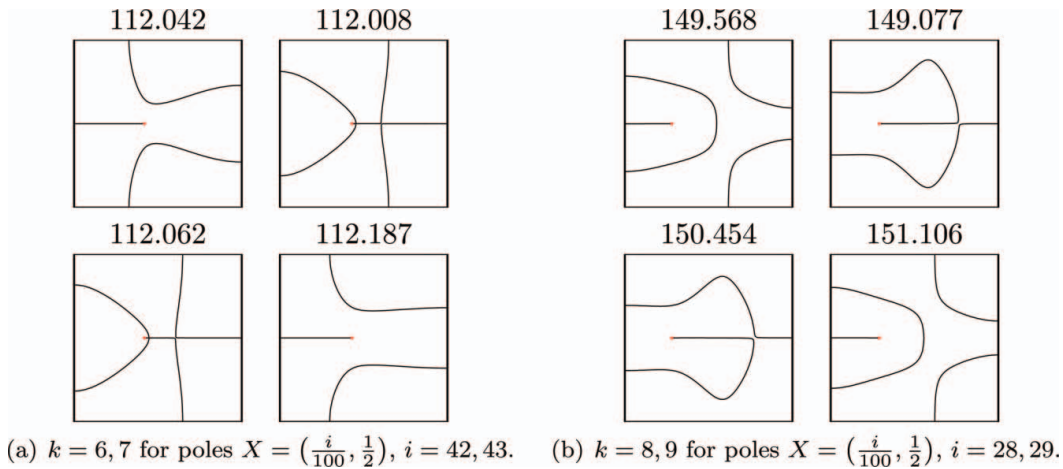


FIGURE 13. Change of symmetry on the nodal sets associated with $\lambda_k^{\text{AB}X(x)}$ (color figure available online).

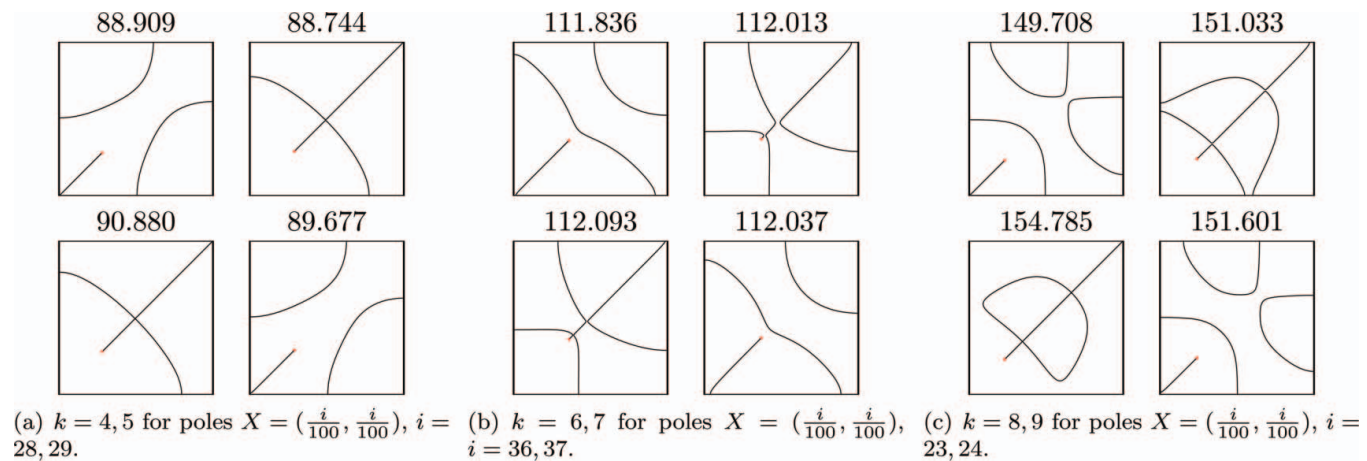


FIGURE 14. Nodal set for the eigenfunctions associated with $\lambda_k^{\text{AB}X}$ (color figure available online).

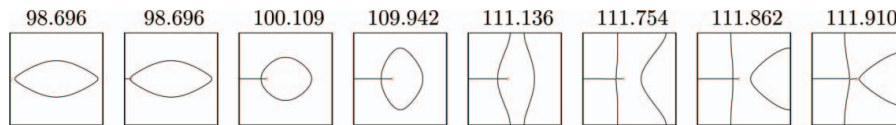


FIGURE 15. Nodal set for the fifth eigenfunction of the **AB**-Hamiltonian with poles $X = (\frac{i}{100}, \frac{1}{2})$, $i = 1, 7, 30, 42, 43, 44, 45, 49$ (color figure available online).

crossing between $\lambda_6^{\text{AB}\tilde{X}(x)}$ and $\lambda_7^{\text{AB}\tilde{X}(x)}$ at $x = c_2$, with $c_2 \in]\frac{36}{100}, \frac{37}{100}[$, and also between $\lambda_8^{\text{AB}\tilde{X}(x)}$ and $\lambda_9^{\text{AB}\tilde{X}(x)}$ at $x = c_3$, with $c_3 \in]\frac{23}{100}, \frac{24}{100}[$. The nodal sets of the corresponding eigenfunctions are given in Figure 14.

Looking at Figures 13 and 14, we can verify that there exists an exchange of symmetry⁴ predicting the existence of the points A_j and C_j .

5.4. Nodal Deformation: An Example

Figure 15 gives the deformation mechanism for the nodal set associated with the fifth eigenvalue of the **ABX**-Hamiltonian for poles $X = (\frac{i}{100}, \frac{1}{2})$, $1 \leq i \leq 50$, on the perpendicular bisector of one side of the square. Between the fourth and fifth subfigures, we have a nodal structure where there are two double points at the boundary.

5.5. Moving the Pole without Respecting the Symmetries of the Square

Figure 16 gives the eigenvalues $\lambda_k(\dot{\Omega}_X^{\mathcal{R}})$ for $1 \leq k \leq 12$ when the pole X belongs to the line $y = \frac{1}{4} + \frac{x}{2}$. We

⁴Look at the horizontal or diagonal nodal line joining the pole to the boundary!

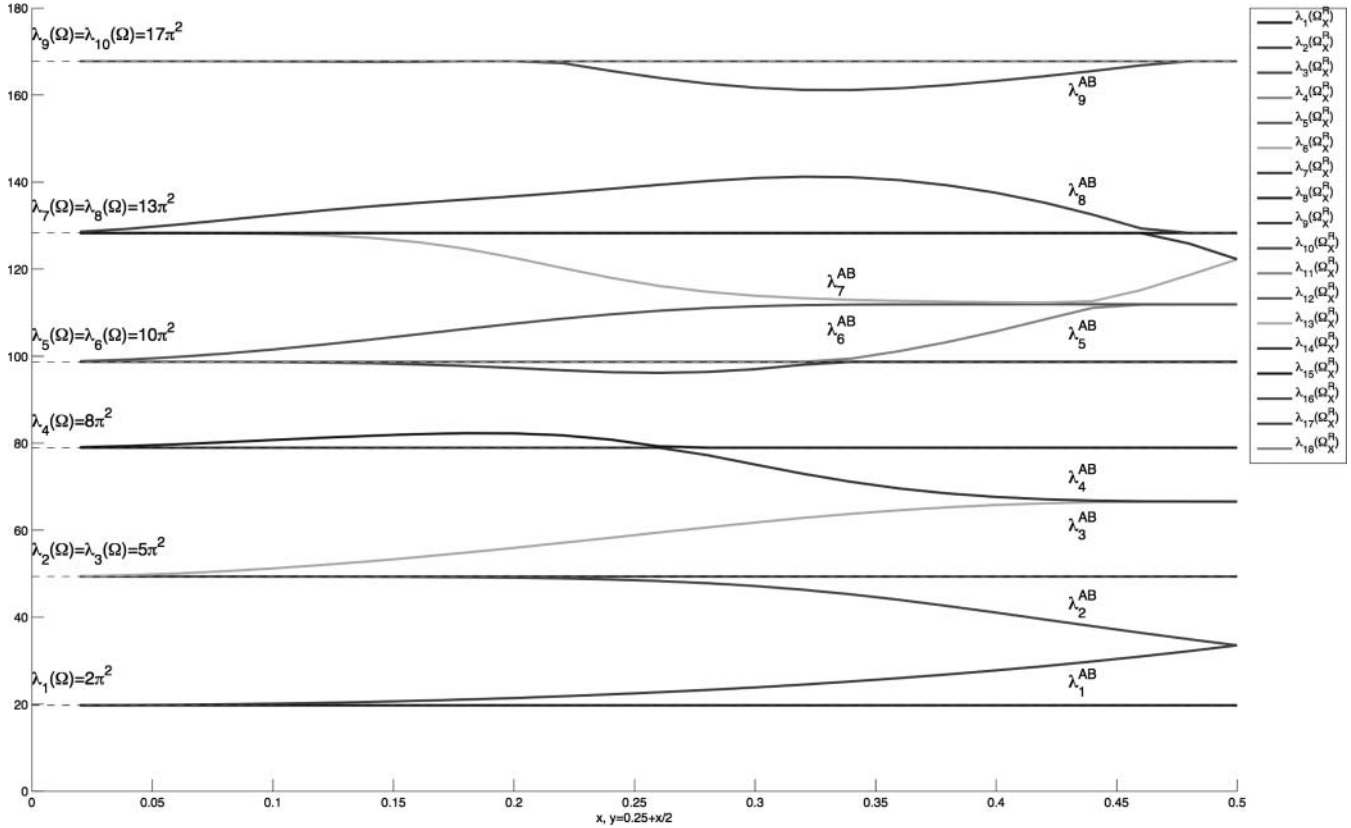


FIGURE 16. Moving the pole along the axis $y = \frac{1}{4} + \frac{x}{2}$, $0 \leq x \leq \frac{1}{2}$.

choose this axis to exhibit a case without symmetry, and we observe that the **AB**-eigenvalues $\lambda_k^{\mathbf{AB}X}$ are no longer monotone with respect to x when $X = (x, \frac{1}{4} + \frac{x}{2})$.

The result should be the same for any arbitrary line (except the perpendicular bisector and the diagonal). We choose to present the simulations for this line, because this line contains enough points in \mathcal{P} to use the previous numerical computations.

It would be interesting to make computations for a finer grid of $X = (x, \frac{1}{4} + \frac{x}{2})$ for x around 0.44 to detect possible crossings between $\lambda_5^{\mathbf{AB}X}$, $\lambda_6^{\mathbf{AB}X}$, and $\lambda_7^{\mathbf{AB}X}$.

6. NODAL SETS AND MINIMAL PARTITIONS

The analysis of $\lambda_5^{\mathbf{AB}X}$ and $\lambda_6^{\mathbf{AB}X}$ leads us to guess numerically the existence of a double eigenvalue when X is the center. As for the pairs $\lambda_3^{\mathbf{AB}X}$ and $\lambda_4^{\mathbf{AB}X}$, which lead us to the family of candidates for the minimal 3-partitions of the square (see Section 4.3), we are led to produce a candidate for a minimal 5-partition for the square, with the property that it is minimal inside the class of 5-partitions that can be lifted to $\hat{\Omega}_C^{\mathcal{R}}$.

Although $\lambda_5^{\mathbf{ABC}} = \lambda_{11}(\hat{\Omega}_C^{\mathcal{R}})$ is not Courant-sharp⁵ for the Dirichlet Laplacian on $\hat{\Omega}_C^{\mathcal{R}}$, we observe that it is Courant-sharp for the **ABC**-Hamiltonian.

This time, neither numerics nor theory gives the existence of a continuous family of 5-partitions. Actually, one knows from elementary results on the perturbation of harmonic polynomials of order 2 that the perpendicular crossing of two lines will generically disappear by perturbation.

In the unit ball of the 2-dimensional eigenspace of $\lambda_{11}(\hat{\Omega}_C^{\mathcal{R}})$ we find only four eigenfunctions, leading to four distinct configurations whose projection on one sheet has five domains. These eigenfunctions are symmetric or antisymmetric with respect to one of the four bisectors of the square (see Figure 17). The other configurations seem to have (see below) four symmetric (for the deck map) pairs of domains. Looking at the linear combination $tu_{11} + (1-t)u_{12}$ of the eigenfunction associated with $\lambda_{11}(\hat{\Omega}_C^{\mathcal{R}})$ and $\lambda_{12}(\hat{\Omega}_C^{\mathcal{R}})$, we observe in Figure 17 that

⁵The index is 11 and not 10.

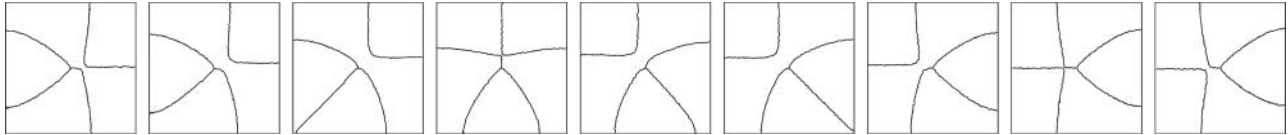


FIGURE 17. Nodal sets of the linear combination of u_{11} and u_{12} $tu_{11} + (1 - t)u_{12}$ with $t = \frac{1}{200}(0, 25, 55, 96, 125, 138, 175, 194, 200)$.

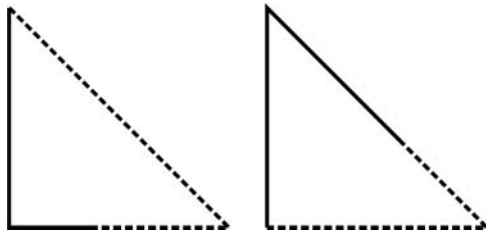


FIGURE 18. Dirichlet-Neumann problem on one-eighth of the square.

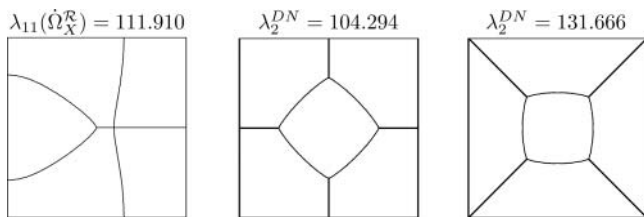


FIGURE 19. Three candidates for the 5-partition of the square.

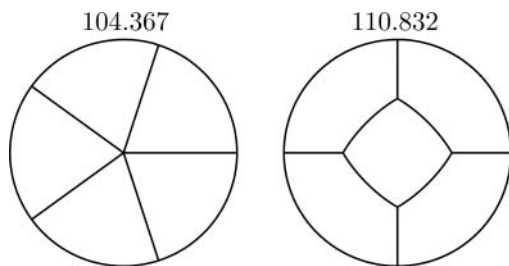


FIGURE 20. Two candidates for the 5-partition of the disk.

the triple point is very unstable and appears only for $t \approx \frac{96}{200}$ and $t \approx \frac{194}{200}$ when we consider $0 \leq t \leq 1$.

Of course it is interesting to compare with what can be obtained by looking at other topological types for the minimal 5-partitions. We recall that these types can be classified using Euler’s formula (see [Helffer and Hoffmann-Ostenhof 10] for the case of 3-partitions). Inspired by [Cybulski et al. 05], we look for a

partition that has the symmetries of the square and four critical points. We get two types of models, and using the symmetries, we can reduce to a Dirichlet–Neumann problem on a triangle corresponding to one-eighth of the square (see Figure 18, where we impose Neumann conditions on dashed lines).

Moving the Neumann boundary on one side as in [Bonnaillie-Noël et al. 10] leads to two candidates. Numerical computations demonstrate a lower energy in one case, which coincides with one of the pictures in [Cybulski et al. 05] (see Figure 19).

Remark 6.1. Note that in the case of the disk a similar analysis leads to a different answer. The partition of the disk by five half-rays with equal angles has a lower energy than the minimal 5-partition with four singular points (see Figure 20). We note that on the basis of standard computations (see, for example, [Helffer et al. 09, (A1) and (A5)]) this energy corresponds to the eleventh eigenvalue of the Dirichlet problem on the double covering on the punctured disk (hence is not Courant-sharp) but corresponds to the fifth eigenvalue of the Aharonov–Bohm spectrum on the punctured disk at the center. Hence it is Courant-sharp in the sense developed in [Helffer et al. 10] (for the sphere), and it shows the minimality of this 5-partition inside the class of the 5-partitions of the disk having a unique critical point that is, in addition, at the center.

7. CONCLUSION

We have explored rather systematically how minimal partitions can be obtained by looking at nodal domains of a problem on the double covering of a punctured square. We have analyzed the behavior of the nodal set in moving the pole in the square. This has permitted us to confirm the status of the “main” candidate for some 3-partitions in the case of the square. This has also permitted us to exhibit a natural candidate for a minimal 5-partition that finally appears to be less favorable than another partition

with four critical points. This is a starting point for a program that can be developed in at least two directions:

- analyze other domains,
- do the same work by considering the double covering of a multipunctured domain and moving the poles.

This program is related to the following conjecture.

Conjecture 7.1. *Let Ω be a simply connected open set of \mathbb{R}^2 . Then*

$$\mathfrak{L}_k(\Omega) = \inf_{\ell \in \mathbb{N}} \inf_{X_1, \dots, X_\ell} L_k^{\mathbf{AB}}(\dot{\Omega}_{X_1, \dots, X_\ell}).$$

Here, for ℓ distinct points $\mathbf{X} = (X_1, \dots, X_\ell)$ in Ω , $L_k^{\mathbf{AB}}(\dot{\Omega}_{X_1, \dots, X_\ell})$ is defined as follows. First we can extend our construction of an Aharonov–Bohm Hamiltonian in the case of a configuration with ℓ points (putting a (renormalized) flux $\frac{1}{2}$ at each of these points). We can also construct (see [Helffer et al. 99]) the antilinear operator $K_{\mathbf{X}}$ and consider the $K_{\mathbf{X}}$ -real eigenfunctions. Here $L_k^{\mathbf{AB}}(\dot{\Omega}_{X_1, \dots, X_\ell})$ denotes the smallest eigenvalue of the \mathbf{AB} - (X_1, \dots, X_ℓ) Hamiltonian for which there is an eigenfunction with k -nodal domains.

Let us present a few examples to illustrate the conjecture. When $k = 2$, there is no need to consider punctured Ω 's. The infimum is obtained for $\ell = 0$. When $k = 3$, it is possible to show that it is enough to minimize over $\ell = 0$, $\ell = 1$, and $\ell = 2$. In the case of the disk and the square, it is proven that the infimum cannot be for $\ell = 0$, and we conjecture that the infimum is for $\ell = 1$ and attained for the punctured domain at the center. For $k = 5$, in the case of the square, it seems that the infimum is for $\ell = 4$ and for $\ell = 1$ in the case of the disk.

Let us explain very briefly why this conjecture is natural. Considering a minimal k -partition, we denote by X_1, \dots, X_ℓ the critical points of the partition corresponding to an odd number of intersecting half-lines. Then we suspect that $\mathfrak{L}_k(\Omega) = \lambda_k^{\mathbf{AB}}(\dot{\Omega}_{X_1, \dots, X_\ell})$ (Courant-sharp situation). Conversely, any family of nodal domains of an Aharonov–Bohm operator on $\dot{\Omega}_{X_1, \dots, X_\ell}$ corresponding to $L_k^{\mathbf{AB}}$ gives a k -partition. Using Euler's formula, see [Helffer and Hoffmann-Ostenhof 10], we obtain easily that the maximal number of critical points with an odd number of intersecting half-lines ℓ is bounded from above by $2k - 3$.

In other words, when the minimal partition is not nodal, we conjecture that it is actually the projection

of a nodal partition of a suitable eigenfunction on the double covering for a suitable puncturing \mathbf{X} .

ACKNOWLEDGMENTS

The authors would like to thank Thomas Hoffmann-Ostenhof, Luc Hillairet, and Susanna Terracini for useful discussions around this topic. We have been particularly stimulated by successive versions of [Noris and Terracini 10]. Discussions about numerics with François Alouges and Grégory Vial were also very fruitful. G. Vial helped us, moreover, by realizing numerous meshes for the computations and also for the detection of the nodal lines.

This paper was partially written during the authors' stay at the Erwin Schrödinger Institute from May to July 2009, and the authors are grateful for the very good working conditions and also for the fruitful discussions with other participants of the workshop Topics in Spectral Theory.

REFERENCES

- [Alziary et al. 03] B. Alziary, J. Fleckinger-Pellé, and P. Takáč. “Eigenfunctions and Hardy Inequalities for a Magnetic Schrödinger Operator in \mathbb{R}^2 .” *Math. Methods Appl. Sci.* 26:13 (2003), 1093–1136.
- [Berger and Rubinstein 99] J. Berger and J. Rubinstein. “On the Zero Set of the Wave Function in Superconductivity.” *Comm. Math. Phys.* 202:3 (1999), 621–628.
- [Bonnaillie-Noël and Helffer 09] V. Bonnaillie-Noël and B. Helffer. “Numerical Analysis of Nodal Sets for Eigenvalues of Aharonov–Bohm Hamiltonians on the Square and Application to Minimal Partitions.” Preprint ESI, 2009.
- [Bonnaillie-Noël and Vial 07] V. Bonnaillie-Noël and G. Vial. “Computations for Nodal Domains and Spectral Minimal Partitions.” Available online (<http://w3.bretagne.ens-cachan.fr/math/simulations/MinimalPartitions>), 2007.
- [Bonnaillie-Noël et al. 09] V. Bonnaillie-Noël, B. Helffer, and T. Hoffmann-Ostenhof. “Aharonov–Bohm Hamiltonians, Isospectrality and Minimal Partitions.” *J. Phys. A* 42:18 (2009), 185203, 20.
- [Bonnaillie-Noël et al. 10] V. Bonnaillie-Noël, B. Helffer, and G. Vial. “Numerical Simulations for Nodal Domains and Spectral Minimal Partitions.” *ESAIM Control Optim. Calc. Var.* 16:1 (2010), 221–246.
- [Bozorgnia 09] F. Bozorgnia. “Numerical Algorithm for Spatial Segregation of Competitive Systems.” *SIAM J. Sci. Comput.* 31:5 (2009), 3946–3958.

- [Conti et al. 03] M. Conti, S. Terracini, and G. Verzini. “An Optimal Partition Problem Related to Nonlinear Eigenvalues.” *J. Funct. Anal.* 198:1 (2003), 160–196.
- [Conti et al. 05a] M. Conti, S. Terracini, and G. Verzini. “On a Class of Optimal Partition Problems Related to the Fučík Spectrum and to the Monotonicity Formulae.” *Calc. Var. Partial Differential Equations* 22:1 (2005), 45–72.
- [Conti et al. 05b] M. Conti, S. Terracini, and G. Verzini. “A Variational Problem for the Spatial Segregation of Reaction–Diffusion Systems.” *Indiana Univ. Math. J.* 54:3 (2005), 779–815.
- [Cybulski et al. 05] O. Cybulski, V. Babin, and R. Holyst. “Minimization of the Renyi Entropy Production in the Space-Partitioning Process.” *Phys. Rev. E (3)* 71:4 (2005), 046130, 10.
- [Helffer and Hoffmann-Ostenhof 10] B. Helffer and T. Hoffmann-Ostenhof. “On Minimal Partitions: New Properties and Applications to the Disk.” In *Spectrum and Dynamics*, Vol. 52, pp. 119–135. Providence, RI: Amer. Math. Soc., 2010.
- [Helffer et al. 99] B. Helffer, M. Hoffmann-Ostenhof, T. Hoffmann-Ostenhof, and M. P. Owen. “Nodal Sets for Groundstates of Schrödinger Operators with Zero Magnetic Field in Non-simply Connected Domains.” *Comm. Math. Phys.* 202:3 (1999), 629–649.
- [Helffer et al. 09] B. Helffer, T. Hoffmann-Ostenhof, and S. Terracini. “Nodal Domains and Spectral Minimal Partitions.” *Ann. Inst. H. Poincaré Anal. Non Linéaire* 26 (2009), 101–138.
- [Helffer et al. 10] B. Helffer, T. Hoffmann-Ostenhof, and S. Terracini. “On Spectral Minimal Partitions: The Case of the Sphere.” *Around the Research of Vladimir Maz’ya III, International Math. Series* 13 (2010), 153–178.
- [Hillairet and Judge 10] L. Hillairet and C. Judge. “The Eigenvalues of the Laplacian on Domains with Small Slits.” *Trans. Amer. Math. Soc.* 362:12 (2010), 6231–6259.
- [Jakobson et al. 06] D. Jakobson, M. Levitin, N. Nadirashvili, and I. Polterovich. “Spectral Problems with Mixed Dirichlet–Neumann Boundary Conditions: Isospectrality and Beyond.” *J. Comput. Appl. Math.* 194:1 (2006), 141–155.
- [Levitin et al. 06] M. Levitin, L. Parnowski, and I. Polterovich. “Isospectral Domains with Mixed Boundary Conditions.” *J. Phys. A* 39:9 (2006), 2073–2082.
- [Martin 07] D. Martin. “MÉLINA, bibliothèque de calculs éléments finis.” Available online (<http://perso.univ-rennes1.fr/daniel.martin/melina>), 2007.
- [Noris and Terracini 10] B. Noris and S. Terracini. “Nodal Sets of Magnetic Schrödinger Operators of Aharonov–Bohm Type and Energy Minimizing Partitions.” *Indiana Univ. Math. J.* 59 (2010), 1361–1402.
- [Shewchuk 05] J. R. Shewchuk. “Triangle: A Two-Dimensional Quality Mesh Generator and Delaunay Triangulator.” Available online (<http://www.cs.cmu.edu/~quake/triangle.html>), 2005.

Virginie Bonnaillie-Noël, IRMAR, ENS Cachan Bretagne, Univ. Rennes 1, CNRS, UEB, av. Robert Schuman, F-35170 Bruz, France (Virginie.Bonnaillie@bretagne.ens-cachan.fr)

Bernard Helffer, Laboratoire de Mathématiques, Bat. 425, Univ Paris-Sud and CNRS, F-91405 Orsay Cedex, France (Bernard.Helffer@math.u-psud.fr)

Received November 19, 2009; accepted June 5, 2010.